



Norwegian University of  
Science and Technology

# Performance and wake measurements of a Savonius wind turbine

**Alexander Dahl Aliferis**  
**Marius Stette Jessen**

Master of Energy and Environmental Engineering

Submission date: June 2018

Supervisor: Robert Jason Hearst, EPT

Co-supervisor: Tania Bracchi, EPT

Norwegian University of Science and Technology  
Department of Energy and Process Engineering



EPT-M-2018-05

EPT-M-2018-41

**MASTER THESIS**

for

Alexander Dahl Aliferis

Marius Jessen

Spring 2018

Performance and wake measurements of a Savonius wind turbine

*Ytelse og vake målinger av Savonius vind turbin***Background**

Vertical Axis Wind Turbines (VAWTs), see Fig. 1a), has historically been a suggested alternative to the most conventional Horizontal Axis Wind Turbine (HAWTs), see Fig. 1b). Despite the VAWTs did not have the same commercial development as HAWTs, there is a growing interest in the use of small VAWTs in urban areas where the wind is highly variable and turbulent [1].

Some of the advantages of VAWT over HAWT are that the performance is independent on the wind direction and low noise emission, which makes VAWTs appealing for urban areas. [2]. This solution would contribute to the growing development in both renewable energy and low-energy demanding buildings.

Nevertheless, the feasibility of wind energy as a resource in urban wind should be investigated further. [3]

Exist two main categories of VAWTs: lift-driven (e.g. Darrieus wind turbine), shown in Fig. 1a), and drag driven (e.g. Savonius wind turbine), shown in Fig. 2).

The Darrieus type rotors are known to be more efficient than the Savonius ones, but the second have the advantage that does not need a start-up device for low wind speeds.

- How VAWTs affect each other when placed in a wind park ?
- Which is the behavior, in terms of production, of VAWTs in highly turbulent flow, as on the roof of a building?

**Objectives**

The present study focuses on the experimental analysis of a Savonius wind turbine. The project is a follow up of the semester project “Performances of vertical axis wind turbines, lift type & drag type”. The objectives are the following:

- Measurement of power and thrust coefficients, for low turbulence in uniform incoming flow, several tip speed ratios and Reynolds numbers
- Measurement of the wake development tens of diameters down-stream
- Measurement of power and thrust coefficients with high turbulence in uniform incoming flow

**The following tasks are to be considered:**

1. Detailed literature review on wake characteristics of VAWTs
2. Improving the existing test rig in the wind tunnel
3. Become familiar with flow and force measurement techniques
4. Perform force measurements in uniform and turbulent incoming flow
5. Perform wake measurements
6. Process data to extract mean and velocity fluctuation information



Figur 1: a) Helicoidal Darrieus wind turbine [4] , b) Horizontal axis wind turbine [5]



Figur 2 Savonius wind turbine [6]

**References**

- [1] Sintef (2013, February 13). *Vindmøller på taket*. Retrieved from <http://www.sintef.no/sistenytt/vindmoller-pa-taket/>
- [2] Balduzzi, Francesco, et al. "Feasibility analysis of a Darrieus vertical-axis wind turbine installation in the rooftop of a building." *Applied Energy* 97 (2012): 921-929.
- [3] Balduzzi, Francesco, et al. "Feasibility analysis of a Darrieus vertical-axis wind turbine installation in the rooftop of a building." *Applied Energy* 97 (2012): 921-929.
- [4] Quora (2017, April). *What is the most efficient design for a Darrieus wind turbine?*. Retrieved from <https://www.quora.com/What-is-the-most-efficient-design-for-a-Darrieus-wind-turbine>
- [5] ETCgreen. *Horizontal axis wind turbine – 1.5MW*. Retrieved from <http://etcgreen.com/products/wind-turbines/horizontal-axis-wind-turbine-1-5mw/>

[6] Eimear Kirby. *Wind Energy*. Retrieved from:  
<http://www.odec.ca/projects/2010/kirbxe2/index.htm>

-- ” --

Within 14 days of receiving the written text on the master thesis, the candidate shall submit a research plan for his project to the department.

When the thesis is evaluated, emphasis is put on processing of the results, and that they are presented in tabular and/or graphic form in a clear manner, and that they are analyzed carefully.

The thesis should be formulated as a research report with summary both in English and Norwegian, conclusion, literature references, table of contents etc. During the preparation of the text, the candidate should make an effort to produce a well-structured and easily readable report. In order to ease the evaluation of the thesis, it is important that the cross-references are correct. In the making of the report, strong emphasis should be placed on both a thorough discussion of the results and an orderly presentation.

The candidate is requested to initiate and keep close contact with his/her academic supervisor(s) throughout the working period. The candidate must follow the rules and regulations of NTNU as well as passive directions given by the Department of Energy and Process Engineering.

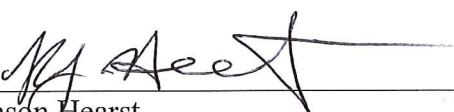
Risk assessment of the candidate's work shall be carried out according to the department's procedures. The risk assessment must be documented and included as part of the final report. Events related to the candidate's work adversely affecting the health, safety or security, must be documented and included as part of the final report. If the documentation on risk assessment represents a large number of pages, the full version is to be submitted electronically to the supervisor and an excerpt is included in the report.


Pursuant to “Regulations concerning the supplementary provisions to the technology study program/Master of Science” at NTNU §20, the Department reserves the permission to utilize all the results and data for teaching and research purposes as well as in future publications.

The final report is to be submitted digitally in DAIM. An executive summary of the thesis including title, student's name, supervisor's name, year, department name, and NTNU's logo and name, shall be submitted to the department as a separate pdf file. Based on an agreement with the supervisor, the final report and other material and documents may be given to the supervisor in digital format.

- Work to be done in lab (Water power lab, Fluids engineering lab, Thermal engineering lab)  
 Field work

Department of Energy and Process Engineering, 12. January 2018

  
\_\_\_\_\_  
Jason Hearst  
Main Academic Supervisor

  
\_\_\_\_\_  
Tania Bracchi  
Co-Academic Supervisor

---

# Acknowledgments

We would like to thank the following persons for their great help and assistance during the completion of this Master thesis:

Our supervisors R. Jason Hearst and Tania Bracchi for your support and guidance throughout the whole project from start to finish. You made a very interesting Master thesis for us and by sharing your knowledge, experience and time you helped us finish it.

Arnt Egil Kolstad, Aslak Brandastrø and the rest of the staff at the laboratory for your contribution in designing, building and setting up the experiment in the wind tunnel. When we experienced technical problems you always had a quick and easy solution. Without your help it would not have been possible to finish the thesis in time.

Bård Brandastrø for your help and support throughout the project, especially in the design phase. You helped us find and order the parts and equipment necessary to perform the experiments.

Lars Morten Bardal for helping us with LabView and various tips and tricks regarding the equipment in the wind tunnel laboratory.

Getek AS in Trondheim for kindly donating the Savonius turbine.

---

# Abstract

In this study, the performance, drag and wake characteristics of a vertical axis Savonius wind turbine are investigated experimentally. The turbine is drag driven and has a helical configuration, making the top rotated 180 degrees relative to the bottom. All experiments were conducted in the wind tunnel at the Norwegian University of Science and Technology. The rotor wake was captured using two Cobra probes produced by Turbulent Flow Industries (TFI). These are 4-holed dynamic pressure probes capable of measuring all three velocity components in turbulent conditions. Both performance and wake measurements were conducted in four different inflow conditions, using Reynolds numbers of  $Re_D \approx 1.6 \times 10^5$  and  $Re_D \approx 2.7 \times 10^5$  and turbulence intensities of 0.6% and 5.7%. The efficiency of the turbine was found to be highly dependent on the Reynolds number of the incoming flow. In high turbulent inflow, the efficiency was only reduced in the case of high Reynolds number. Hence, greater levels of turbulence results in a weaker Reynolds number dependency of the rotor performance. The drag of the turbine was shown to be independent of the turbines rotational speed over the range tested, and it was slightly lower in high turbulent inflow.

The wake was captured for the described inflow conditions in both optimal and sub-optimal operating conditions by varying the rotational speed of the turbine. Measurements were conducted in a horizontal plane at the center height of the turbine, spanning 2.3 turbine diameters in both lateral directions relative to the turbine center-line, and up to 11.6 diameters downstream of the turbine. Results show an asymmetrical wake formation in optimal operating conditions where the velocity deficit is greatest behind the returning turbine blade. In sub-optimal conditions, the wake is more symmetric. Regarding levels of turbulent kinetic energy in the wake, a proportionality with the inflow turbulence intensity was observed.

The levels of lateral entrainment in the far wake (above 8 diameters downstream) are found to increase in high turbulence, This leads to more turbulent mixing and faster recovery of the far wake. In low Reynolds number flow, higher inflow turbulence intensity increase the wake width compared to the case of almost uniform inflow. This is in contrast to the wakes of horizontal axis wind turbines. The opposite effect was however observed in high Reynolds number flow. Based on the findings from the wake measurements, some recommendations on where to place supplementary turbines.

---

# Sammendrag

I denne oppgaven undersøkes ytelsen, drag-kraften og vakeegenskapene til en vertikal-akse Savonius-type vindturbin, basert på eksperimentelt utførte forsøk. Turbinen er drevet av drag-krefter og har en vridd konfigurasjon, slik at toppen er rotert 180 grader i forhold til bunnen. Alle eksperimentene i oppgaven er gjennomført i vindtunnelen til Norges Teknisk-Naturvitenskapelig Universitet. Vaken til turbinen er målt med to Cobra prober produsert av Turbulent Flow Industries (TFI). Disse er 4-hullede dynamiske trykkprober, som er i stand til å måle alle tre hatighetskomponenter i turbulente forhold. Både ytelses- og vakemålinger ble utført i forskjellige innstrømningsforhold med Reynolds-tall på  $Re_D \approx 1.6 \times 10^5$  og  $Re_D \approx 2.7 \times 10^5$ , samt turbulensintensitet på 0.6% og 5.7%. Effektiviteten til turbinen viste seg å være svært avhengig av Reynolds-tallet til den innkommende vindstrømmen. Økt turbulensintensitet medførte en lavere virkningsgrad for høyt Reynolds-tall, noe som tilsier at virkningsgradens Reynoldsavhengighet minker når turbulensintensiteten øker. Drag-kraften på turbinen var uavhengig av rotasjonshastigheten over det testede operasjonsintervallet, og den ble observert som noe lavere ved høyturbulent innstrømning.

Vaken til turbinen ble kartlagt i de forskjellige innstrømningsforholdene beskrevet ovenfor, samt ved både optimal og sub-optimal drift av turbinen med tanke på rotasjonshastighet. Målinger ble utført i et horisontalt plan ved midten av turbinens høyde, der planet strekker seg med 2.3 turbindiametere i begge laterale retninger i forhold til turbinens midtlinje, og opp til 11.6 diametere nedstrøms for turbinen. Resultatene viser en asymmetrisk vakedannelse under optimale driftsforhold og en mer symmetrisk vake under sub-optimale forhold. Det ble også påvist en proporsjonalitet mellom turbulent kinetisk energi i vaken og turbulensintensitet i den innkommende strømmingen.

Nivåene av lateral turbulent moment-fluks etter 8 diametere nedstrøms for turbinen, øker tilsynelatende med høyturbulent innstrømning. Dette fører til økt turbulent miksing i denne regionen og konsekvent raskere gjenoppsettelse av vaken. I vindstrømning med lavt Reynolds-tall, gir høy turbulens i motsetning til horisontal-akse vindturbiner, en tykkere vake sammelignet med en uniform innstrømningsprofil. Det motsatte ble dog observert ved høyt Reynolds-tall i vindstrømmen. Basert på funnene i vakemålingene, er det avslutningsvis kommet med enkelte forslag til plassering av supplerende Savonius turbiner.



---

# Table of Contents

<b>Acknowledgments</b>	<b>i</b>
<b>Abstract</b>	<b>ii</b>
<b>Sammendrag</b>	<b>iii</b>
<b>Table of Contents</b>	<b>v</b>
<b>1 Introduction</b>	<b>1</b>
<b>2 Experiment</b>	<b>5</b>
2.1 Experimental Setup . . . . .	5
2.1.1 Turbine . . . . .	5
2.1.2 Inflow Conditions . . . . .	6
2.2 Measurement Methods . . . . .	7
2.2.1 Performance measurements . . . . .	7
2.2.2 Wake measurements . . . . .	8
2.2.3 Measurement Uncertainties . . . . .	9
<b>3 Wind turbine performance</b>	<b>11</b>
3.1 Power and Torque Coefficients . . . . .	11
3.2 Drag Coefficient . . . . .	14
<b>4 Wake measurements</b>	<b>17</b>
4.1 Velocity Deficit . . . . .	17
4.2 Wake turbulence . . . . .	19
<b>5 Time series analysis</b>	<b>23</b>
<b>6 Conclusion</b>	<b>25</b>
<b>Bibliography</b>	<b>27</b>
<b>Appendices</b>	<b>31</b>
<b>A More on the experimental set up</b>	<b>33</b>
<b>B Additional Contour Figures</b>	<b>37</b>
<b>C Turbulence Decay</b>	<b>41</b>

---

## List of Figures

2.1	Schematic of the experimental setup in the wind tunnel, seen from above.	5
2.2	Images of the set up in the wind tunnel . . . . .	6
2.3	Schematic of the set up in the wind tunnel (seen from the side) . . . . .	7
2.4	Measurement grid seen from above. . . . .	9
3.1	Power coefficient, $C_P$ . . . . .	11
3.2	Torque coefficient, $C_M$ . . . . .	12
3.3	Drag coefficient, $C_D$ . . . . .	14
4.1	Normalized mean streamwise velocity component . . . . .	17
4.2	Development of wake thickness . . . . .	18
4.3	Contours of normalized time-averaged turbulent kinetic energy $k$ . . . . .	19
4.4	Lateral momentum flux . . . . .	20
4.5	Vertical momentum flux . . . . .	21
5.1	Normalized spectrum of streamwise velocity fluctuations, $u'$ . . . . .	24

## List of Tables

2.1	Inflow Conditions . . . . .	7
2.2	Settings for the different wake measurements . . . . .	9
3.1	Power Coefficient, $C_P$ . . . . .	12
3.2	Average drag coefficient, $C_D$ . . . . .	15

---

# 1. Introduction

The world's demand for renewable energy is rapidly increasing. With the development of "greener" cities and the establishment of zero- and plus-energy buildings, this demand goes beyond large-scale electrical production systems such as offshore wind- and hydro-power. The implementation of smart grid systems in cities and other densely populated areas comes with an expectation of more on-site electrical production systems. An alternative to the already well-developed and widely used rooftop-photovoltaic-systems is urban wind power. However, wind conditions in urban areas are highly variable, turbulent and characterized with low mean velocities [Kumara et al. (2017)]. Thus, they are far from optimal for traditional horizontal axis wind turbines (HAWTs). The performance of vertical axis wind turbines (VAWTs), is on the other hand, known to be less influenced by these environmental factors, leading to recent commercial investigation and development of VAWTs in the application of urban wind power. VAWTs are generally divided into two main groups, lift driven and drag driven. Within these two categories of turbines, the drag driven Savonius turbine has the advantage of good self-starting abilities and peak performance at low rotational velocities, the latter adding the additional benefits of low noise emissions and less danger if a structural malfunction should occur. While lift-type VAWTs also have their benefits, the present study will focus on Savonius type turbines for these reasons.

There have been several papers published on the performance of Savonius turbines. Blackwell et al. (1978) found a Reynolds dependency of the turbine performance in wind tunnel experiments. The Reynolds number is generally in VAWT literature and in this report given by

$$Re_D = \frac{\rho U_\infty D}{\mu}, \quad (1.1)$$

where  $\rho$  is the density,  $U_\infty$  is the incoming velocity,  $\mu$  is the viscosity and  $D$  the turbine diameter. Blackwell et al. (1978) however, described their flow conditions with Reynolds number per meter [ $Re = \rho U_\infty / \mu$ ], with values of  $4.32 \times 10^5$  and  $8.67 \times 10^5$ . A similar Reynolds dependency was reported by Damak et al. (2013) for a Savonius with helical twist operating in a Reynolds number ( $Re_D$ ) range of  $7.97 \times 10^4$  to  $1.47 \times 10^5$ . The twisted configuration was also proven to increase the efficiency by Saha and Rajkumar (2006). Different performance characteristics for different Reynolds numbers in uniform flow were also measured by the authors of the present study in a previous report [Aliferis and Jessen (2017)]. This dependency was highest for Reynolds numbers between  $8.61 \times 10^4$  to  $2.61 \times 10^5$ . Reynolds numbers above  $2.61 \times 10^5$  gave very small changes in the performance.

Akwa et al. (2012) presented a review of studies on Savonius rotors and stated that the performance also has a large dependency on the aspect ratio, buckets spacing, buckets overlap, number of rotor stages, buckets and rotor shapes, shaft and other accessories such as end plates. For example, both end plates and high aspect ratio are found to increase the performance as the effects of "bucket" tip losses are reduced.

In the investigation of VAWTs in urban environments, it is of great interest to map their performance in turbulent conditions. Loganathan et al. (2017) measured the effect

---

of different turbulence intensities on the power output of a Savonius micro-turbine with 24, 30 and 40 blades operating under a range of wind speeds. The turbulence intensities ranged from 1.8% to 17%. There are few reports on similar experiments for more conventional two-bladed Savonius turbines, both with and without helical twist. Some comparable results have however been simulated by Akwa (2010) using the finite volume method for turbulence intensities of 1% and 10%. All results show a negative impact on the performance with increasing turbulent intensity. These findings are interesting as they are potentially opposite to those of HAWTs. As stated by Bardal and Sætran (2017), HAWT power output is increased with increasing turbulence intensity for operating conditions far below rated wind speed. The opposite trend was however stated when the turbine operates in conditions closer to the rated wind speed. The conventional representation of performance is with the coefficient of power defined by

$$C_P = \frac{P}{\frac{1}{2}\rho AU_\infty^3}, \quad (1.2)$$

where  $P$  is the turbine output power and  $A$  is the projected frontal area of the turbine. Following Bardal and Sætran (2017), values of  $C_P$  will either increase or decrease with the turbulence intensity. To exclude these dependencies, a turbulence equivalent wind-speed which can replace  $U_\infty$  in Equation 1.2, was proposed by Rozenn et al. (2008) and Choukulkar et al. (2015). The reports by Loganathan et al. (2017) and Akwa (2010) do not mention any use of this turbulence equivalent windspeed. It was neither quoted in the review summary of Savonius turbines by Akwa et al. (2012).

In addition to investigation of performance with different turbulence intensities, the response of the Savonius turbine to wind gusts have been evaluated by Marmutova (2016). She found that the performance-dependency on tip-speed ratio was reduced with increasing gust frequency.

For structural considerations, it is important to investigate the drag force acting on the turbine. Fujisawa and Gotoh (1994) analyzed the differences in drag force with respect to the tip-speed ratio defined as

$$\lambda = \frac{\omega R}{U_\infty} \quad (1.3)$$

where  $\omega$  is the turbine rotational velocity and,  $R$ , radius of the turbine. They found the time-averaged drag on the Savonius turbine to be independent of the tip speed ratio at values above 0.4. Experiments by Alder (1979) support this conclusion. They also found the drag coefficient given by

$$C_D = \frac{F_D}{\frac{1}{2}\rho AU_\infty^2} \quad (1.4)$$

where  $F_D$  is the drag force, to take values of about one for Reynolds numbers between  $2 \times 10^5$  and  $6 \times 10^5$ . Both of these studies are however limited to the case of low turbulence intensity. A report that does compare laminar and turbulent inflow has been made by Pol (2015). The results are however obtained using CFD, for a single Reynolds number and a constant rotational speed of the turbine. The turbulence intensity of the inflow is not specified. Nevertheless, Pol found the drag coefficient to decrease from 1.29 to 1.21 with

---

an increase of turbulent inflow.

Another important aspect in the urban application of vertical wind turbines, is the development of the wake formation downstream of the rotor. Knowledge on the fluid dynamic wake behavior is important for the arrangement of multiple turbines in limited space. It is also valuable in the optimization process of different blade configurations. Torresi et al. (2014) obtained the unsteady flow field for different angular positions downstream of a 2-bladed Savonius rotor using hot-wire anemometry. The report focused on blade optimization rather than turbine array configuration, so the wake measurements are however bound to a distance of  $x/D \approx 1.2$  ( $x$  being the streamwise coordinate) behind the rotor. In contrast, Shigetomi et al. (2011) examined the flow field around a single Savonius rotor as well as an array of two turbines for optimal configuration. They visualized the flow field using particle image velocimetry, and obtained values of both streamwise and cross-stream velocities up to  $x/D \approx 3$ . The results showed that there were four specific arrangements of the array that gave superior performance relative to that of a single turbine. The arrangements utilizes the fact that the wake of Savonius turbines is asymmetrical. By evaluating the frequency spectrum of streamwise velocity fluctuations, Shigetomi et al. (2011) found two evident peaks at frequencies equal to one- and two-times the cyclic frequency of the turbine. The peak at the lowest of these frequencies, was associated to the shedding of a single vortex in a unit rotation of the turbine. The possible formation of a staggered vortex street downstream of the turbine was also mentioned as a possible explanation to this inner peak, while the outer was coupled to the passage of the two turbine “buckets”. Further analysis on turbine interaction using CFD was done by Zhang et al. (2017) with an increased number of turbines and a more detailed investigation of the turbulent kinetic energy in the wake. They found that one of the optimal array configurations stated by Shigetomi et al. (2011) was superior to the others. The optimal layout is achieved by placing downstream secondary turbines on the advancing blade side, outside the wake of prior turbines. This layout is a result of the wake being detrimental to downstream turbines, and because the wake asymmetry makes it possible to place the turbines closer on the advancing blade side for a given area.

Reports on wakes in hydro-kinetic applications of Savonius are also comparable. Brammer et al. (2013) compared CFD-results with experimental data for the average wake velocity of a Savonius tidal stream turbine. Their results showed good agreement between the simulated and measured values. A more comprehensive wake study for different Reynolds numbers with CFD, and some description of turbulent behavior in the wake has been carried out by Kumar and Saini (2017). The report does however focus on the effects of twist angle on the overall performance and not on wake recovery. Each of these reports on hydro-kinetic application of a Savonius turbine are only based on one constant value of turbulence intensity of 10% and 5%, respectively.

In 2012, SINTEF [Haase et al. (2014)] placed out a number of helical Savonius turbines on one of Oslo’s tallest buildings (Biskop Gunnerus Gate 14) to obtain correlations between wind measurements, electricity production and noise. They concluded among other things that wake aspects of wind resources in the built environment are poorly understood and that further development work is necessary to exploit the full potential of the



---

studied Savonius turbine in urban wind application.

The present study, aims to improve our understanding of the wake and aerodynamic performance with low and high levels of turbulence intensity. This is in contrast to most previous studies that have been performed using a single level of turbulence intensity at the inflow. Even though some of the reports have looked at the effects of turbulence on the power output and efficiency, they have not directly compared any Reynolds dependency to that of almost uniform inflow. In addition to the investigation of the wake with different initial flow conditions, our study intends to give a better analysis of the wake and its recovery under different operating conditions. This includes the assessment of lateral and vertical turbulent momentum transport in the wake, which is common in studies of wake recovery for horizontal-axis wind turbines (HAWTs) and Darrieus type VAWTs [Tian et al. (2014), Shamsoddin and Porté-Agel (2017)]. To perform these analyses, all components of the wake velocity in the horizontal plane have been measured using two dynamic 4-hole pressure probes to a position  $x/D = 11.6$  downstream of the turbine. The two chosen Reynolds numbers for measurements of both performance and wakes in this report, are based on results of  $C_P$ -dependency on Reynolds number from our previous study on the same Savonius turbine. For wake measurements, two different  $\lambda$  were chosen to represent optimal and far below optimal operating conditions of the turbine.

## 2. Experiment

### 2.1 Experimental Setup

All the experiments were conducted in the low-speed closed-loop wind tunnel in the fluid mechanics lab at the Norwegian University of Science and Technology. The test section of the wind tunnel is 11 m long, 2.71 m wide and 1.81 m high. To counteract wall boundary layer growth the height of the ceiling is gradually increased to 1.85 m through the test section. This is the same tunnel used by Bartl and Sætran (2017).

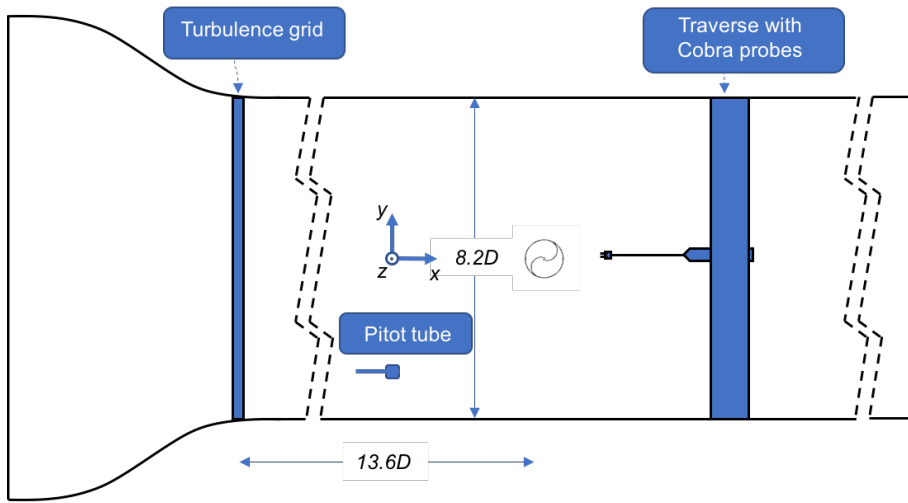


Figure 2.1: Schematic of the experimental setup in the wind tunnel, seen from above.

#### 2.1.1 Turbine

The Savonius turbine in this study has a helical twist where the top is rotated 180 degrees relative to the bottom. It is also equipped with end plates. The turbine has diameter,  $D = 0.33\text{m}$ , is 0.99 meters tall and a projected frontal area of  $A = 0.327\text{ m}^2$ . For all measurements, the turbine was placed  $x/D = 13.6$  or 4.5 meters downstream of the test section inlet.

With the turbine inside the tunnel, the blockage is 9.86 %. Velocities are corrected for the blockage effect of the turbine using Pope and Harper's correction method:

$$U_c = U_\infty \left( 1 + \frac{S}{4A_t} \right) \quad (2.1)$$

where  $S$  is the model blocked area and  $A_t$  the wind tunnel area, following the procedure described by Ross (2010).

---

## 2.1.2 Inflow Conditions

Turbine performance and wake characteristics are investigated for four different inflow conditions in this study. The conditions are changed by having either uniform or turbulent inflow and using two different Reynolds numbers of  $Re_D \approx 1.6 \times 10^5$  and  $Re_D \approx 2.7 \times 10^5$ , which corresponds to velocities of  $U_\infty \approx 7.8$  m/s and  $U_\infty \approx 13.9$  m/s respectively.



**Figure 2.2:** Set up in the wind tunnel. *Left:* Uniform inflow with additional support struts connecting the turbine to the ceiling. *Right:* Turbulent inflow with grid at the inlet of the test section.

The total velocity is decomposed into three velocity components where  $U$  is the velocity in the x(streamwise)-direction,  $V$  in the y(cross-streamwise)-direction and  $W$  is the velocity component in the z(vertical)-direction. In order to analyze the turbulent statistics of the wind, all of the velocity components are defined so that

$$U = \langle U \rangle + u'. \quad (2.2)$$

Here,  $U$  is the instantaneous velocity component,  $\langle U \rangle$  is the time-averaged (mean) velocity component while  $u'$  is the time-varying velocity fluctuation. By defining the velocity in this manner, the turbulence intensity may be calculated as

$$I = \frac{\sqrt{\langle u'^2 \rangle}}{\langle U \rangle}. \quad (2.3)$$

The turbulence intensity of the incoming flow is varied by placing a turbulence-inducing grid at the inlet of the wind tunnel. See Figure 2.2 for reference. The grid is made of wooden bars with  $47\text{mm} \times 47\text{mm}$  cross-section and has a mesh size of  $M = 0.245\text{m}$ , resulting in a solidity of 35%. Introducing the grid to the flow induced considerable variations in the horizontal velocity profile of the incoming flow, however the variation over the turbine diameter was within 1.5%. Similar observations were made by Bartl and Sætran (2017) who used the same grid. The different inflow conditions are summarized in Table 2.1.

Test Case #	Turbulence Grid	Reynolds number $Re_D$	Turbulence intensity $I[\%]$
1	No	$1.6 \times 10^5$	0.6
2	No	$2.7 \times 10^5$	0.6
3	Yes	$1.5 \times 10^5$	5.7
4	Yes	$2.7 \times 10^5$	5.7

**Table 2.1:** Inflow Conditions

## 2.2 Measurement Methods

### 2.2.1 Performance measurements

The turbine power production can be calculated by  $P = M \cdot \omega$ . Here,  $M$  is the torque produced by the turbine which is measured using a HBM torque transducer of the type T20W-N/5-Nm. The rotational velocity,  $\omega$ , is found by measuring the number of turbine rotations per minute,  $n$ , with an optical RPM sensor and the relation  $\omega = \frac{2\pi n}{60}$ . Further, a Siemens three-phase Squirrel-Cage-Motor with rated power of 550 W, was used as a generator in the experiments. All of the mentioned equipment were used by Bartl and Sætran (2017).

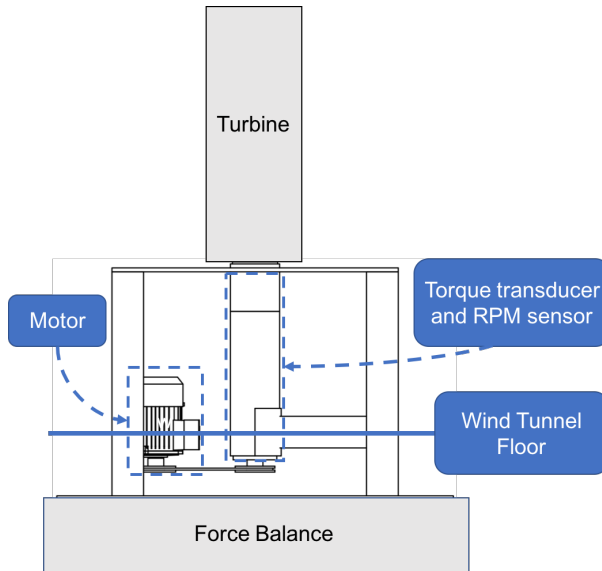


**Figure 2.3:** Schematic of the set up in the wind tunnel, seen from the side (Not to scale).

Similar to the expressions given in Equation 1.2 and 1.4, the torque coefficient is defined as

---


$$C_M = \frac{M}{\frac{1}{2}\rho AU_\infty^2} \quad (2.4)$$

The density is calculated from ideal gas law, using the current temperature measured by a thermocouple. The incoming velocity is calculated from the dynamic pressure, measured with a Pitot tube placed in front of the turbine. In an effort to reduce the influence of considerable vibrations in the system, the turbine was attached to the ceiling during the measurements of  $C_P$  and  $C_M$  with additional supports struts.

The drag force is measured using one load cell on a six-component force balance produced by Carl Schenck AG. Again, this component has been used in previous experiments at the same facility, e.g by Bartl and Sætran (2017). In order to remove the drag force contribution from the support structure, the drag force was measured under all inflow condition without the turbine. The drag force of the turbine itself was then isolated as,

$$F_D = F_{D_{total}} - F_{D_{support}} \quad (2.5)$$

The turbine and support structure was only mounted to the plate on the balance when capturing the drag force.

For all performance measurements, the sampling rate was 1000 Hz and the sampling time was 30 seconds. The performance of the turbine was captured in all the different flow conditions by varying the turbine rotational speed using the mentioned Siemens induction motor controlled by a frequency converter. The energy generated by the turbine was dissipated in a small electric heater.

## 2.2.2 Wake measurements

The wakes behind the turbine were measured using two Cobra Probes produced by Turbulent Flow Instrumentation (TFI). Cobra Probes are 4-holed dynamic pressure probes, capable of measuring all three velocity components and local static pressure in real time. These probes were also used to measure the incoming velocity profiles and turbulence intensities for the empty tunnel. Draskovic (2017) investigated the accuracy of these probes compared with laser Doppler anemometry and hot wire anemometry, and concluded that the Cobra probes were suitable for measurements in complex turbulent flows. The stated expected error in mean velocities under 10 m/s and high ambient turbulent conditions was about 2%. Further, the maximum expected error in turbulence intensity was 1%, but in most cases it was not more than 0.6%.

Figure 2.4 illustrates the measurement grid. The grid is uniformly spaced with  $\Delta y = 3$  cm between each measurement point. There are fifteen such scans distributed downstream of the turbine, with the last measurements at  $x/D = 11.6$ . The necessary grid spacing was found by performing an initial scan and investigating the resolution of the velocity components. In the z-direction, the measurement plane is located at the center of the turbine height. The sampling frequency was 1250 Hz for all the measurements, which was sufficient to compute the mean turbulence statistics. For the measurements at the lowest

Reynolds number, the sampling time was 60 seconds while a sampling time of 30 seconds was used for the highest Reynolds number. Some longer measurements of 120 seconds were taken in locations of high turbulence for spectral analysis.

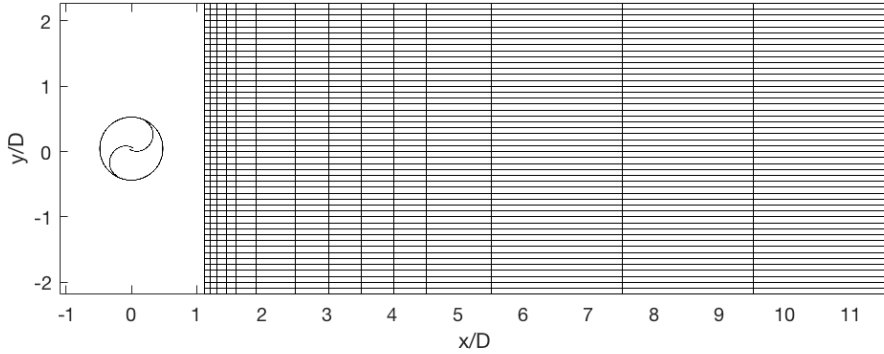


**Figure 2.4:** Measurement grid seen from above. Here,  $x$  is the distance from the turbine center in the streamwise direction and  $y$  is the horizontal cross-streamwise direction.  $y = 0$  represents the center of both the turbine and the wind tunnel.

The wake behind the turbine was captured under the four inflow conditions described in Table 2.1 and two different operating conditions. The operating condition of the turbine was altered by changing the tip-speed ratio of the turbine. A summary of the different test cases is depicted in Table 2.2. For all cases, the mean U-component,  $U_0$  across the span

Test Case #	Turbulence Grid	Reynolds number $Re_D$	Tip-speed Ratio $\lambda$
A	No	$1.7 \times 10^5$	0.8
B	Yes	$1.7 \times 10^5$	0.8
C	No	$2.7 \times 10^5$	0.8
D	Yes	$2.8 \times 10^5$	0.8
E	No	$1.7 \times 10^5$	0.4
F	Yes	$1.6 \times 10^5$	0.4

**Table 2.2:** Settings for the different wake measurements

of the wake in the first streamwise position ( $x/D = 1.12D$ ) is used as the normalizing velocity.

### 2.2.3 Measurement Uncertainties

The uncertainties in the measurements of performance were calculated as described by A. J. Wheeler (2004). Random statistical errors are computed in a 95% confidence interval for all measured parameters. Systematic errors originating from the calibration procedures

---

are also accounted for. The total error in each measured variable is calculated as the root-sum-square of the random and systematic errors.

For each of the calculated variables  $C_P$ ,  $C_M$ ,  $C_D$  and  $\lambda$  the error is found by the law of error propagation using the total error in each dependent parameter. All of the performance variables are plotted with their respective uncertainties and the mean relative error of each measurement series is presented as well.

The accuracy of the Cobra probes is quoted from the manufacturer to be dependent on the turbulence level. Generally, it should be within  $\pm 0.5$  m/s and  $\pm 1^\circ$  in pitch and yaw angles (used to calculate velocity components) up to about 30% turbulence intensity. The conditions in this study are generally well below this limit and thus the uncertainty is below the aforementioned values. In regions of very high turbulence intensity, i.e. near the turbine, the accuracy of the measurements is somewhat lower. The quoted accuracy from the manufacturer together with the stated expected errors by Draskovic (2017), make the Cobra probes acceptable for the purpose of the experiments followed by this report.

Empty wind tunnel investigations showed that the turbulence intensity decays by up to 27 % from the first to the last measurement point 11.6 diameters downstream of the turbine center. A more detailed description of the decay in turbulence intensity is given in Appendix C.

### 3. Wind turbine performance

#### 3.1 Power and Torque Coefficients

The coefficients of power,  $C_P$ , and torque,  $C_M$ , were calculated as in Equation 1.2 and Equation 2.4, respectively, using the measured average torque and the blockage corrected velocity. Averaged values of the coefficient of power,  $C_P$ , and their associated uncertainties, are plotted in Figure 3.1 for the described inflow conditions. By inspecting the figure, a clear increase in both the magnitude and the tip-speed ratio, of the maximum power coefficient  $C_{P_{max}}$  for increasing  $Re_D$  is evident. Interestingly, the impact of turbulence intensity appears to reduce  $C_P$  in high Reynolds number inflow only. Hence, the Reynolds number dependency of  $C_P$  in turbulent inflow is weaker. This reduction in dependency can somewhat be quantified by a difference in  $C_P$  at  $\lambda = 0.7$  of 44% and 48% for high and low turbulence, respectively. Further, an attempt of using the proposed equivalent windspeed by Choukulkar et al. (2015) and Rozenn et al. (2008) in the calculation of  $C_P$  and  $\lambda$ , did not result in any noticeable changes to the plots in Figure 3.1.

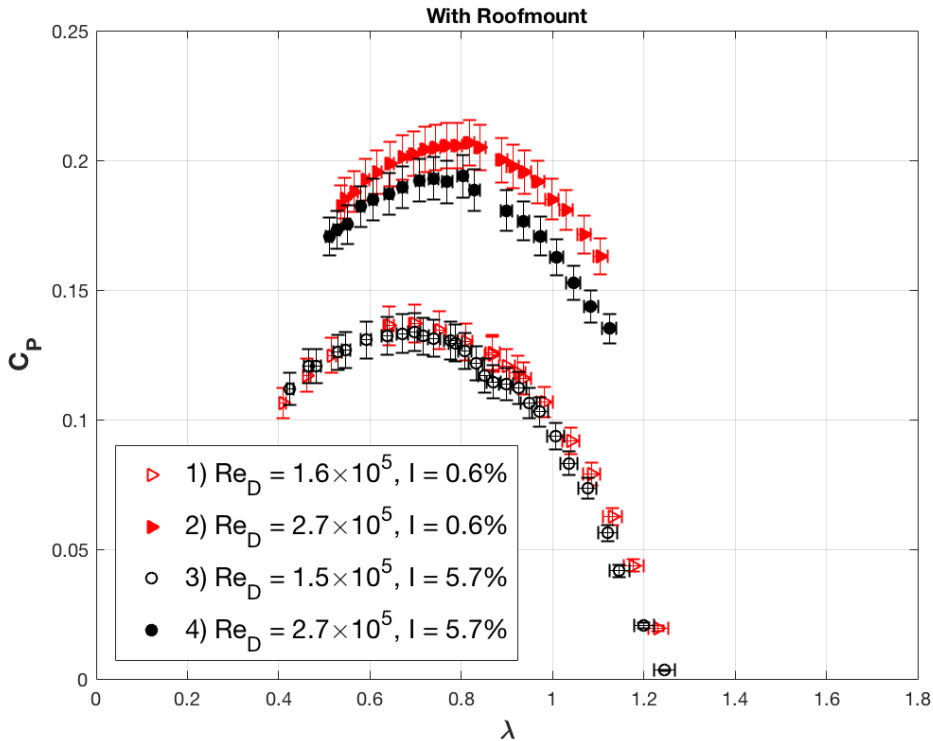


**Figure 3.1:** Power coefficient,  $C_P$ , as a function tip speed ratio,  $\lambda$ , for the Savonius turbine. Plotted with uncertainties in both variables.



Test Case #		Inflow conditions		Power Coefficient	
		$Re_D$	$I$ [%]	$C_{Pmax}$	Mean Error
1	▷	$1.6 \times 10^5$	0.6	0.1370	$\pm 3.4\%$
2	▶	$2.7 \times 10^5$	0.6	0.2067	$\pm 4.3\%$
3	○	$1.5 \times 10^5$	5.7	0.1336	$\pm 4.4\%$
4	●	$4.3 \times 10^5$	5.7	0.1939	$\pm 4.4\%$

**Table 3.1:** Power Coefficient,  $C_P$

Figure 3.2 which depicts the torque coefficient,  $C_M$ , as a function of the tip speed ratio shows the same tendency. Also apparent in Figure 3.2, is a linear decrease in the torque coefficient with increasing tip-speed ratio. This phenomenon was also observed by Damak et al. (2013), who measured torque and power coefficients on a Savonius turbine with a helical twist angle of 180 degrees.

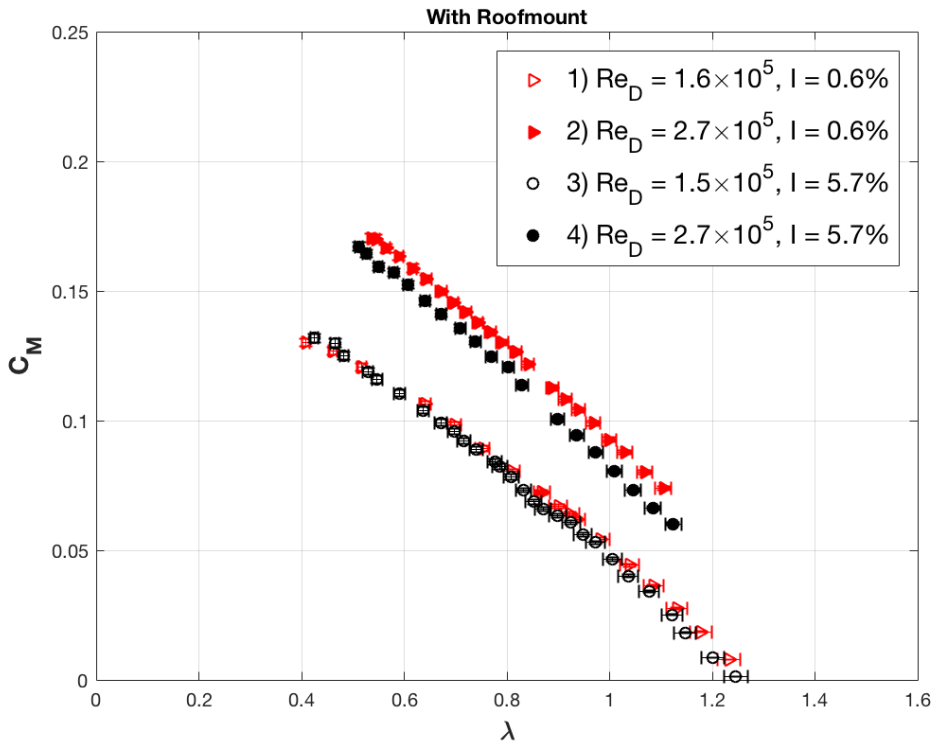


**Figure 3.2:** Torque coefficient,  $C_M$ , as a function tip speed ratio,  $\lambda$ , for the Savonius turbine. Plotted with uncertainties in both variables.

Blackwell et al. (1978), who experimented on conventional Savonius turbines, suggested

---

that the observed Reynolds number dependency is due to delay of flow separation for high  $Re_D$  on the convex side of the rotor buckets, induced by the transition to a turbulent boundary layer. This phenomenon is especially significant when the rotor has an angular position near  $0^\circ$  and  $180^\circ$  (i.e the edge of either bucket is facing the incoming flow). At these angles, the flow characteristics on the facing bucket is substantially similar to flow around a cylinder. When the boundary layer becomes turbulent and separation is delayed, the pressure drag on the returning bucket is reduced. This is because of the increased pressure recovery on the concave side of the bucket. As the pressure drag on the returning bucket at those angular positions reduces, the torque is increased. Because the turbine in question has a helical twist, there are more angular positions in a rotation where a "bucket" is facing the wind. The helical geometry then increase the effect described above, causing an even stronger Reynolds number dependency. This theory is supported by the fact that the data obtained by Blackwell et al. (1978) on conventional Savonius turbines with no helical twist, shows a weaker Reynolds number dependency than that observed here. Damak et al. (2013), who performed experiments on a Savonius turbine with an helical twist, also observed a stronger Reynolds number dependency compared to the study by Blackwell et al. (1978). A summary of the maximum value and the mean error in of the power coefficient for all four cases is summarized in Table 3.1. For the torque coefficient, the errors are small and all within 1%.

Even though the motor used in the experiments did not provide enough torque to obtain values of  $C_M$  for tip-speed ratios lower than 0.4, the trend of  $C_M$  increasing as  $\lambda$  decreases in Figure 3.2 is very positive regarding self-starting abilities. Lastly, the values of  $C_{P,max}$  can be regarded as very satisfying as they are in the upper range compared to of values reported by Akwa et al. (2012). Resulting uncertainties are also quite low and in well agreement with uncertainties obtained by Blackwell et al. (1978). Therefore, these data can confidently be considered conclusive.

---

## 3.2 Drag Coefficient

Figure 3.3 depicts the drag coefficient,  $C_D$ , as a function of tip speed ratio for the Savonius turbine. Here, the measured drag force is normalized as in Equation 1.4 and adjusted for the drag of the support structure.

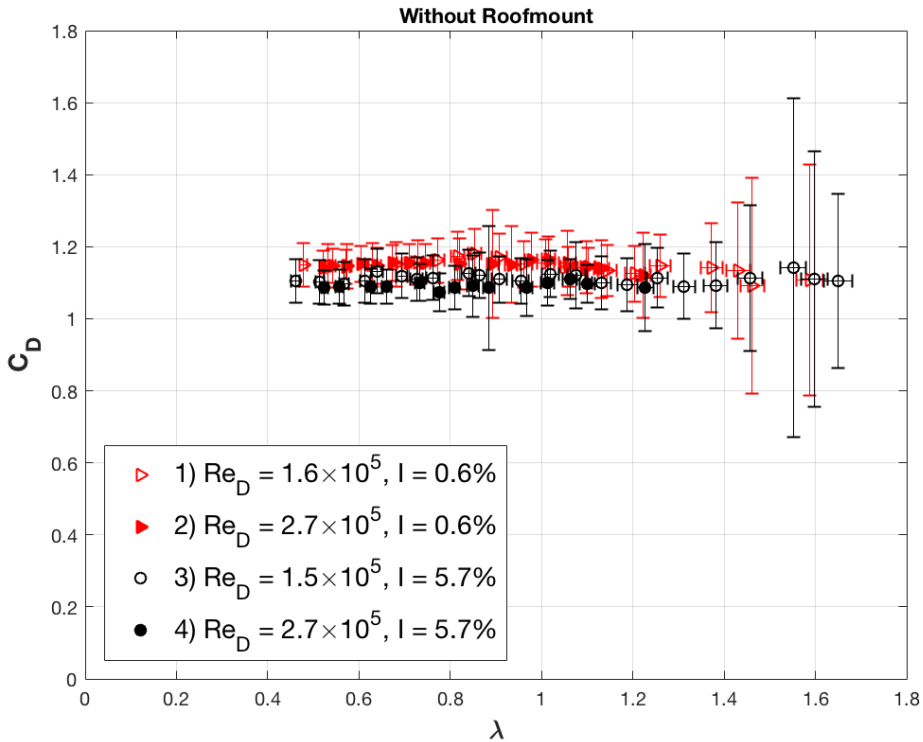


**Figure 3.3:** Drag coefficient,  $C_D$ , as a function tip speed ratio,  $\lambda$ , for the Savonius turbine with uncertainties in both variables.

The drag coefficient shows little dependency on  $\lambda$ . This tendency is supported by drag measurements from other Savonius experiments e.g Fujisawa and Gotoh (1994). They further found the drag coefficient only to vary significantly at tip-speed ratios below 0.4, thus leading to the thought that blade blockage effect is the dominant or only source of drag force on Savonius turbines. Blade blockage is simply the effect of the blades preventing the flow from passing through the turbine's swept area because they are solid, which results in an increased drag force when the turbine rotates faster. As the Savonius turbine has very small gaps where air can pass through it, this blockage effect can reach a maximum value at quite low rotational speeds.

---

Averaged values of  $C_D$  over the ranges of tip-speed-ratios are summarized in Table 3.2. The values of  $C_D$  are similar between Reynolds numbers, but a slight decrease is observed in high turbulent inflow. Pol (2015) who performed CFD analysis on a Savonius turbine using both laminar and turbulent simulation models, reported similar findings. This phenomenon may perhaps be explained by comparing the results to the familiar case of a cylinder in cross flow. A previous study performed by Bell (1979) showed that increasing the turbulence intensity in the incoming flow up to 5% induces reduction in  $C_D$  for a cylinder. This is because the intensity of perturbations in the boundary layer increases, causing the separation points to move backwards and reducing the pressure drag. A similar effect may be evident for the Savonius turbine as well.

Test Case #		Inflow conditions		Drag Coefficient	
		$Re_D$	$I$ [%]	$C_{D_{mean}}$	Mean Error
1	▷	$1.6 \times 10^5$	0.6	1.1463	$\pm 8.9\%$
2	▶	$2.7 \times 10^5$	0.6	1.1489	$\pm 6.0\%$
3	○	$1.5 \times 10^5$	5.7	1.1112	$\pm 10.4\%$
4	●	$2.7 \times 10^5$	5.7	1.0908	$\pm 6.5\%$

**Table 3.2:** Average drag coefficient,  $C_D$



## 4. Wake measurements

### 4.1 Velocity Deficit

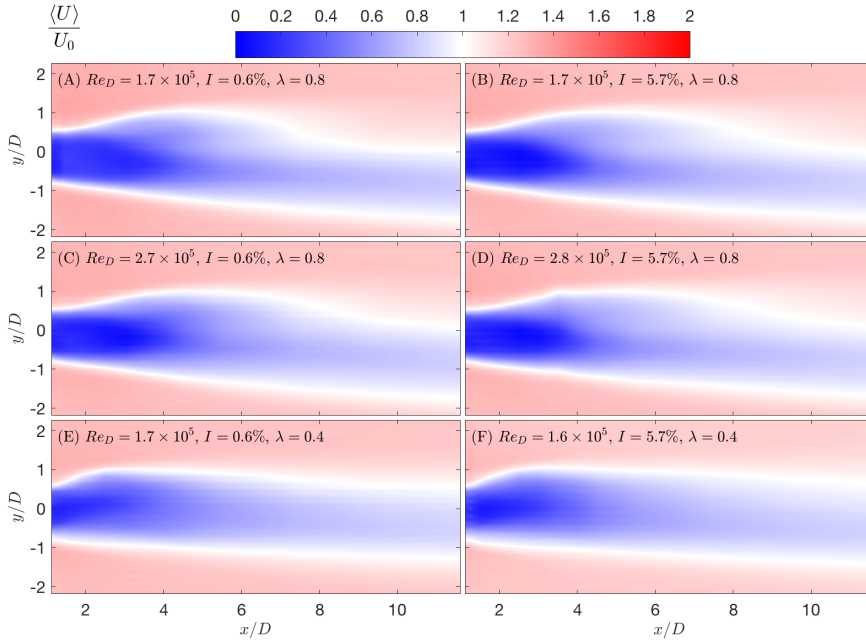
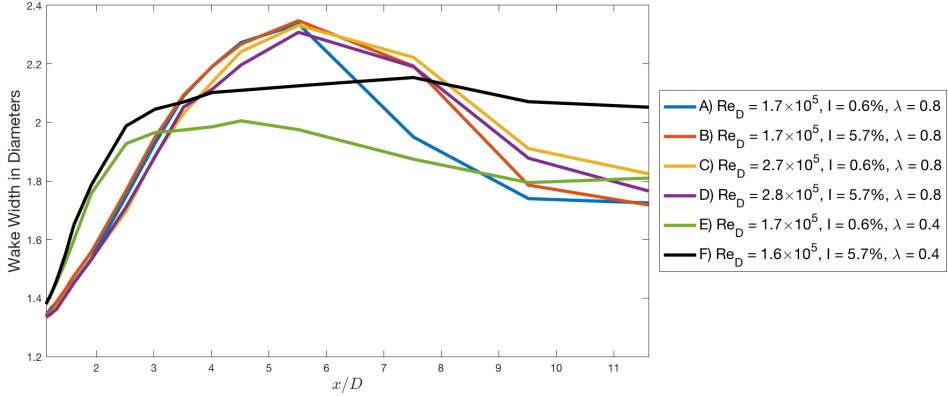


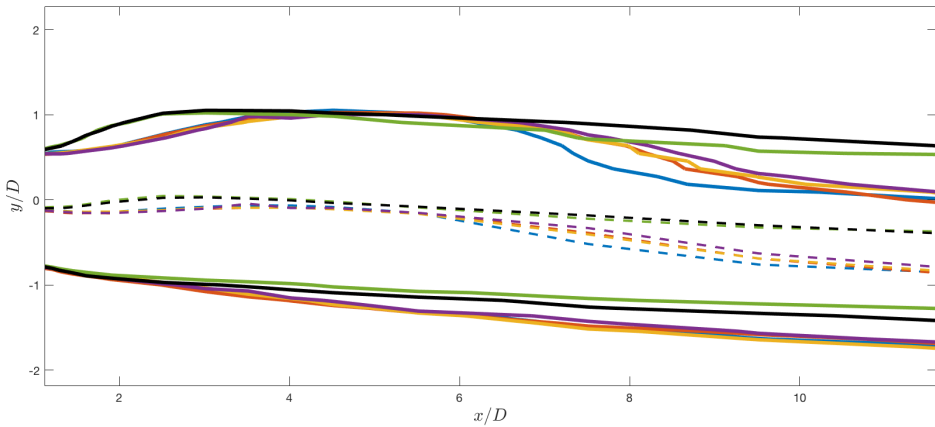
**Figure 4.1:** Contours of normalized time-averaged streamwise velocity of the wake in the x-y plane

The normalized time-averaged streamwise velocity,  $\langle U \rangle / U_0$  is illustrated in Figure 4.1. For all cases, there is a highly visible velocity deficit behind the turbine. This deficit is positioned more predominantly toward  $y/D < 0$ , which results in an asymmetric wake. The wake is asymmetric because the returning blade is of more significant obstruction to the incoming flow than the advancing blade. For easier discussion, regions of  $y/D < 0$  and  $y/D > 0$  will hereinafter be referred to as the strong and weak side of the wake, respectively. Further, by evaluating the wake width given in Figure 4.2a and 4.2b, there are quite large deviations for the different types of inflow and operating conditions. In the cases of low Reynolds numbers, the wake is wider for high incoming turbulence intensity (TI), at least in the downstream region of  $x/D > 5.5$  up to  $x/D \approx 11$  for optimal  $\lambda$ , and  $x/D > 2$  for sub-optimal  $\lambda$ . This is in contrast to results from experiments on HAWTs obtained by Tian et al. (2014). At sub-optimal operating conditions i.e low  $\lambda$ , the increase in wake width with turbulence intensity, is highest and more persistent downstream of the rotor. This can be explained by the airflow on the turbine blades having more similarities with airflow on a sharp-edged disc when the relative velocity of the turbine to the incoming flow is reduced. Rind and Castro (2012) reported that the boundary layer separation point on a sharp edged disc remains unchanged with inflow TI, and that stronger TI increases the

disc wake deficit and width. This is in contrast to flow around a sphere or cylinder where stronger TI delays separation, and hence reduce the wake deficit and width. For higher Reynolds numbers the mentioned relation between TI and wake width is reversed in the whole range of  $x/D$ , although with fewer observed differences with the inflow TI.



(a)



(b)

**Figure 4.2:** (a) Development of thickness (distance between lines of  $\langle U \rangle / U_0 = 1$ ) of the wake. (b) Contours of  $\langle U \rangle / U_0 = 1$  for all test cases. The dashed lines depicts the center-line of the wake.

Plots of  $\langle V \rangle$  and  $\langle W \rangle$  velocity components are attached in Appendix B. The values in these plots compared to that of Figure 4.1 are very small, and they seem non-intuitive as they do not tend to zero in the far wake. Since the values in the plots are small, measurement errors can be considered as very influential on both  $\langle V \rangle$  and  $\langle W \rangle$ . The corresponding fluctuations however, with proper normalization, should be uninfluenced by measurement errors in the mean. Hence, obtained values of the normalized fluctuations in all directions are considered conclusive.

## 4.2 Wake turbulence

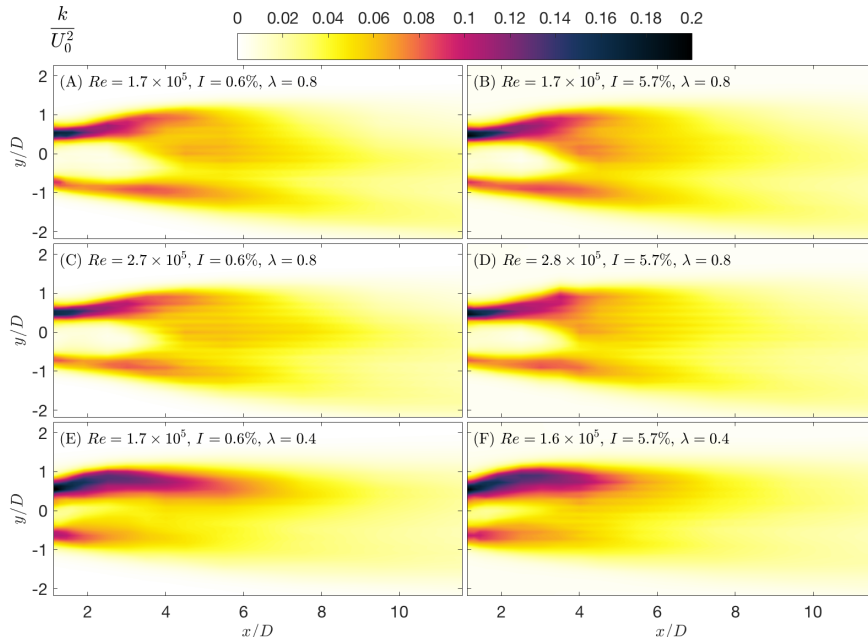


**Figure 4.3:** Contours of normalized time-averaged turbulent kinetic energy,  $k$ , in the  $x$ - $y$  plane of the wake

The turbulent kinetic energy in the wake (TKE) is given by

$$k = \frac{1}{2} [\langle u'^2 \rangle + \langle v'^2 \rangle + \langle w'^2 \rangle], \quad (4.1)$$

and depicted in Figure 4.3. For all cases, the TKE is highest in the region behind the advancing turbine blade. It is likely that increased torque generation by the advancing blade, (which represents almost all the total torque generation by the turbine) has a positive correlation with TKE as more torque generation will cause a greater disturbance in the flow. This is visible by comparing cases (A) and (B) to (E) and (F) in Figure 4.3, with the increased generation of torque for lower  $\lambda$  depicted in Figure 3.2. Interestingly, the turbulent kinetic energy on the strong side of the wake is lower in the cases of high Reynolds number. The reduction in the peak value of TKE with respect to increased Reynolds number is here 8.28% and 9.27% for the cases of low and high turbulence intensity, respectively. As found by Schaffarczyk et al. (2018), flow separation increases production levels of TKE. Thus, the explanation of increased efficiency due to less flow separation on the returning blade for higher Reynolds number is in good agreement with this observed reduction of TKE. Comparing the results of different inflow TI, the spatial distribution of large TKE levels seems to increase for high TI. These larger values are especially evident towards  $y/D = 0$ . Peak values of TKE are however more or less unchanged, although



they are more concentrated with low inflow TI. Without a more detailed study of the air-flow through the turbine, it is difficult to obtain a certain reason for this increased spatial distribution of large TKE values with high inflow TI. A simple but perhaps appropriate explanation might be the fact that more turbulent flow passes through the turbine in a given time period.

Contributions from the streamwise, cross-streamwise and vertical fluctuations to the turbulent kinetic energy are attached in Appendix B.

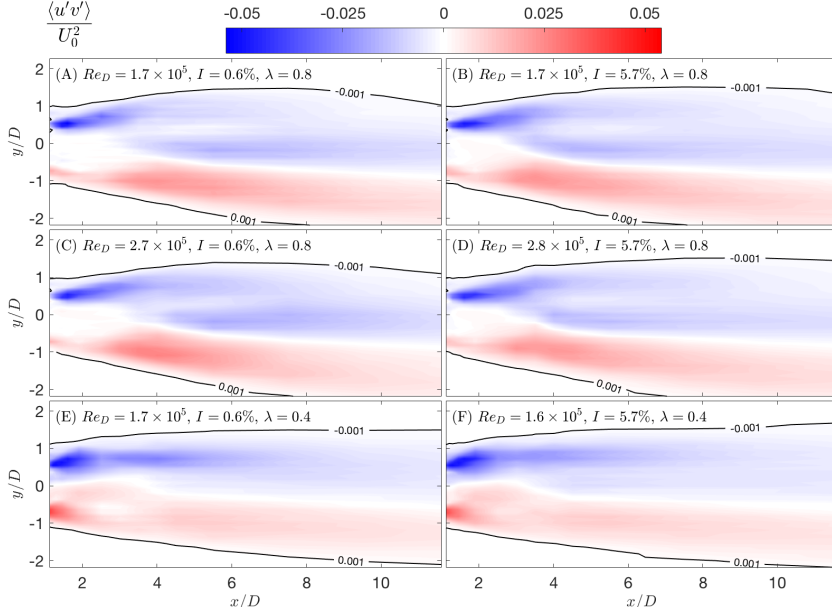


**Figure 4.4:** Normalized contours of lateral momentum flux  $\left(\frac{\langle u'v' \rangle}{U_0^2}\right)$

In the literature of wind turbine wakes, it is common to inspect the turbulent momentum fluxes as they quantify flow entrainment into the wake. Figure 4.4 shows the normalized values of lateral momentum flux for the different cases. For all cases there are two regions, one of positive and one of negative flux, that transfer energy from the outer flow into the wake. The levels of these entrainments are however quite dependent on the tip-speed ratio. Near the optimal operating conditions of  $\lambda = 0.8$ , the momentum flux on the weak side of the wake is dominant. The highest levels of entrainment in the strong side of the wake is also farther downstream. Interestingly, in the near wake ( $x/D < 4$ ) the entrainment from the strong side extends less towards the middle for case (A) than in the other cases. To somewhat quantify this, the measured turbulence momentum flux in case (B) which has the second lowest value at  $x/D = 3.5, y/D = 0.36$ , is 107% larger than in case (A). This is in agreement with the center-line of the wake in case (A) depicted in Figure 4.2b, being more deflected towards the strong side. The mentioned effect of less entrainment in this region is delayed in terms of  $\langle U \rangle$ , and is hence observable farther downstream e.g  $x/D > 6$ . The absolute values of turbulent momentum flux are almost equal in magnitude and despite the

described deviation above, the fluxes in the near wake are very similar regardless of the Reynolds number. With lower operating  $\lambda$ , the levels of entrainment becomes much more evenly distributed, which results in a more symmetric wake.

The most evident difference created by the increased levels of TI is in the farthest regions of the wake ( $x/D > 8$ ), especially on the weak side. The lateral span of this region is increased by about 10%  $\sim$  20% between the different cases for increased levels of turbulence inflow. By the lower black contour line in Figure 4.4, it is also observable that there is a small increase in the lateral span of entrainment in the strong side of the wake as well. The effect of larger entrainment regions in the far wake with high inflow TI is relatable to the development in wake width of the mean velocity field as shown in Figure 4.2a. The difference in wake width in the case of sub-optimal  $\lambda$  is reduced in this same region. Thus, increased inflow TI induces a higher rate of wake recovery for all cases in the far wake, due to more turbulent mixing with high TI. This can be substantiated by the slope of the curves for high inflow TI in Figure 4.2a, being negative for  $x/D > 9$ .

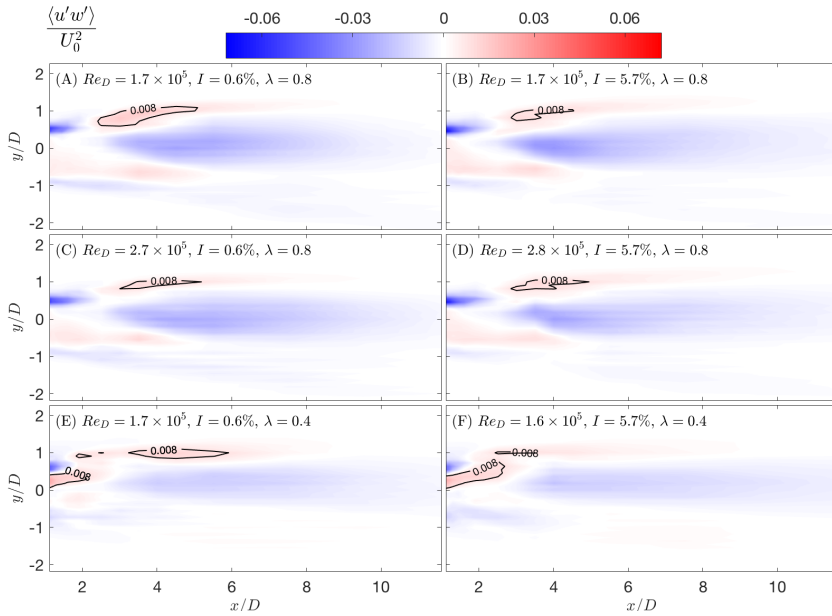


**Figure 4.5:** Normalized contours of vertical momentum flux  $\left(\frac{\langle u'w' \rangle}{U_0^2}\right)$ . Black contour lines are added for vertical entrainment levels of 0.008 in the weak side of the wake

Vertical momentum flux is depicted in Figure 4.5. In optimal operating conditions, i.e.  $\lambda = 0.8$ , there are two distinct regions of upward entrainment. The positive region in the strong side of the wake is absent in the remaining cases of low  $\lambda$ . By the black contour lines mapping the positive entrainment in the weak side of the wake, it is observable that there is more turbulent momentum flux with low inflow TI and low Reynolds number. In the case of high Reynolds number, there is an opposite relation between the levels of TI and momentum fluxes. This specific region of positive entrainment in the weak side of the wake has again a delayed effect in terms of mean velocities and is likely the

---

source of the increased wake recovery at  $x/D > 6, y/D > 0$  seen in Figure 4.1. As stated by Shamsoddin and Porté-Agel (2017) who performed horizontal wake studies on a Darrieus type turbine, it is necessary to have a vertical scan of the wake to further explain the behavior of vertical turbulence momentum flux. Without such a scan, it is also not possible to confidently draw relations between drag and wake measurements either.

## 5. Time series analysis

Normalized spectral analysis of the wake measurements are given in Figure 5.1, where  $f_T = n/60$ . Similar to Shigetomi et al. (2011), there are two peaks of the streamwise fluctuations at frequencies of one and two times the turbine rate of rotation. The latter peak is a result of the two-bladed structure of the turbine, as a point in the circumference is passed twice by a blade per unit rotation. The inner peak suggests that a single vortex is shed once during a complete rotation. This peak could however, be related to the formation of a vortex street behind the turbine. Following Frikha et al. (2016)'s CFD-study on incidence angle effect on the turbulent kinetic energy, the vortex shedding from the returning and advancing blade does not coincide. The collision and interaction of these shed vortices can thus produce a staggered vortex street in the wake. The fact that the observed inner peak is most noticeable and of greater magnitude in the wake region of  $x/D > 1.41$ , is in very good agreement with the possible formation of a vortex street.

It should be kept in mind that the different operating conditions induce differences in the characteristics of the wake. As seen in Figure 4.3, the spatial distribution of TKE and hence peak fluctuations are different for the given inflow conditions. This redistribution is obvious when comparing results in the spectra for different operating tip-speed ratio, as the strongest fluctuations are measured farther downstream in the wake for the reduced  $\lambda$ . These fluctuations are also significantly stronger as the advancing blade is expected to produce more torque and hence increasingly disturb the flow. By the point-wise spectrum representation in Figure 5.1, it is difficult to identify specific effects of increased TI and Reynolds number. In some instances, values are reduced. In others, values are increased. These mixed results are likely related to the explained spatial differences in wake fluctuations for the different operating conditions.

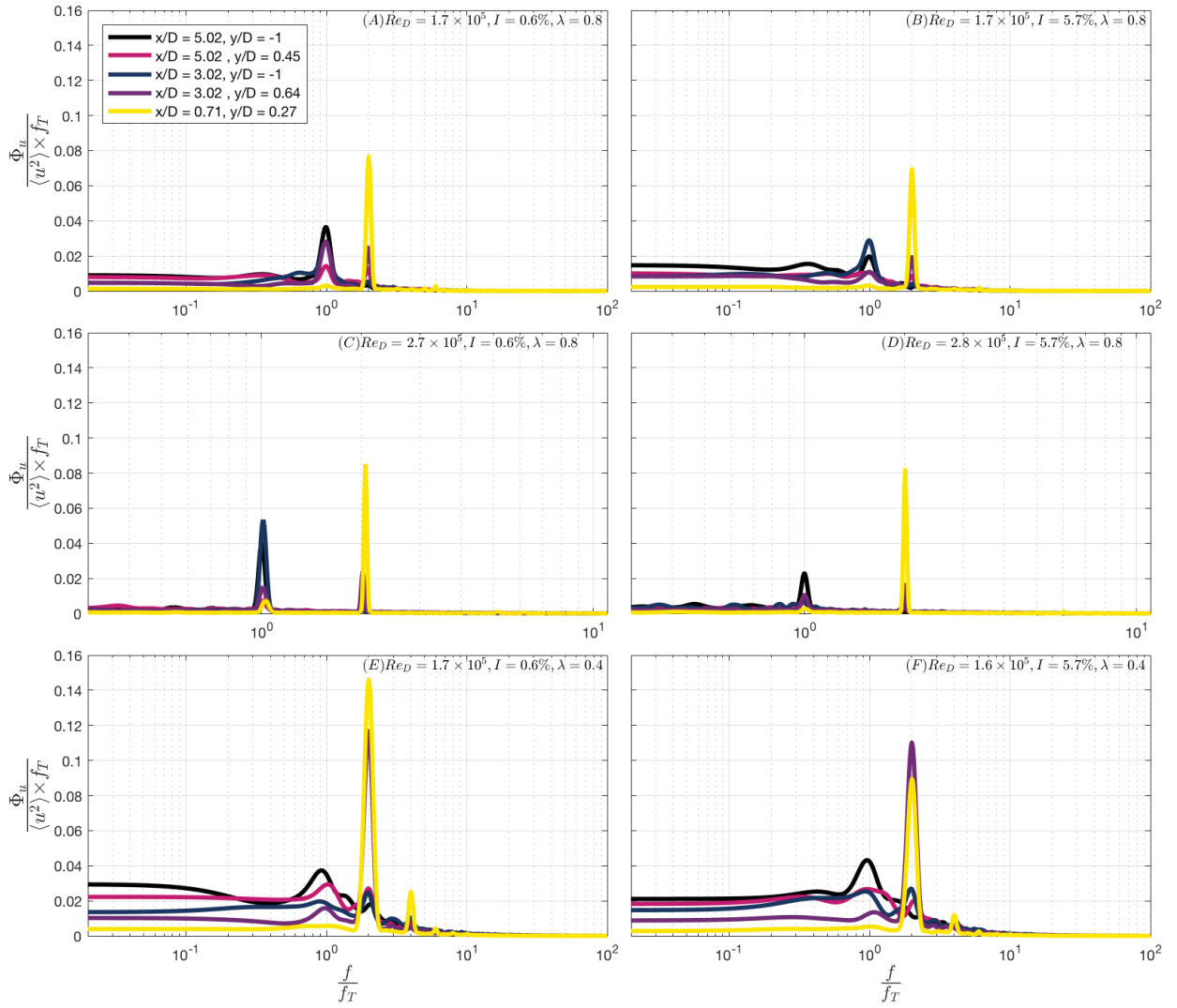


**Figure 5.1:** Normalized spectrum of streamwise velocity fluctuations,  $u'$

## 6. Conclusion

In this study, measurements of the aerodynamic performance and the wake of a Savonius wind turbine for both high and low Reynolds number and inflow turbulence intensity have been conducted. The chosen Reynolds numbers were based on a previous experiment on the same turbine, as the performance was found to be highly dependent on this non-dimensional quantity.

Similar to Akwa et al. (2012), results of the measurements show that the power coefficient decreases with higher inflow turbulence intensity. This decrease was however only observable for the highest Reynolds number. Thus, the  $Re_D$ -dependency of the power coefficient is reduced as the turbulence is increased. The drag coefficient showed little dependency on  $\lambda$ , and a slight decrease was found for higher inflow turbulence intensity. This finding is also supported in CFD simulations performed by [Pol (2015)]. Compared to the case of a cylinder in cross flow with high incoming flow turbulence intensity, this effect can perhaps be explained with less flow separation around the turbine.

The detailed study of the wake in the different turbine operating conditions described above shows an asymmetrical behavior of the wake. Time-averaged analysis indicates that the largest velocity deficit occurs behind the returning turbine blade. The measured asymmetry was noticeably dependent on  $\lambda$  and the largest asymmetry was observed for the case of low Reynolds number and wind turbulence intensity. In contrast to the results of HAWTs, the wake width of the Savonius turbine was found to increase with low Reynolds number and turbulent inflow. The opposite effect was however observed for high Reynolds number. A proposed similarity of the airflow on the turbine blades as the turbine is sub-optimally operated, and airflow on a sharp-edged disc with a fixed separation point is also quoted.

As turbine torque production depends on the rate of kinetic energy extraction from the wind, greater torque production will cause larger disturbances to the incoming flow. Hence, there is an expected proportionality between turbine torque production and higher levels of TKE in the wake. A proportionality was also found between wake TKE and levels of inflow turbulence intensity. This effect was merely attributed to the fact that more turbulent flow passes through the turbine in a given time period with higher wind TI.

Lateral and vertical turbulent momentum flux are characterized as very important for wake recovery and re-energization. Deviations in resulting values of lateral entrainment in high and low incoming turbulence intensity are however less apparent, especially in the near wake. When both the turbulence intensity and the Reynolds number of the incoming flow are low, the spatial extension towards the middle of the wake is smaller. Lowering  $\lambda$  for the turbine creates larger differences. Similar to the time-averaged velocity results, the levels of lateral entrainment becomes much more symmetric. In the far wake for all levels of  $\lambda$ , stronger inflow intensity increases the span of the lateral turbulent momentum fluxes. The vertical entrainment is likely the source of increased wake recovery in the far weak side region of the wake. To give any further explanation of the vertical momentum fluxes, a vertical wake scan is necessary and should thus be investigated in a future study.

---

Finally, with the specified wake characteristics described above, it is possible to give some insight on the optimal placement of supplementary Savonius turbines. Due to the blockage of incoming wind by the first rotor, there are two downstream regions of high time-averaged streamwise velocities outside the wake. As the wake is asymmetric, the accelerated region on the weak side is considered to be optimal. To get the most out of the blockage effect, a second turbine should not be placed too far downstream either. Although previously believed to increase overall efficiency, placement of a second turbine with the returning blade in the strong side wake of the upstream turbine was proven to be inefficient by Zhang et al. (2017). They proposed a different layout where the second turbine is placed outside the upstream turbine wake, providing an accelerated incoming velocity profile similar to that of the leading turbine. The coordinates for this location was given by Zhang et al. (2017) to be  $x/D \approx 5.80, y/D \approx 2.40$ . Based on the result of this report, the optimal location should remain unchanged considering the different inflow conditions of both high and low Reynolds number and TI. The given optimal position will neither be affected by lower  $\lambda$ .

# Bibliography

- A. J. Wheeler, A. R. G., 2004. Introduction to Engineering Experimentation, 3rd Edition. Pearson Education, chap. 7.
- Akwa, J. V., 2010. Análise aerodinâmica de turbinas eólicas savonius empregando dinâmica dos fluidos computacional. Master's thesis, Universidade Federal do Rio Grande do Sul. Escola de Engenharia. Programa de Pós-Graduação em Engenharia Mecânica.
- Akwa, J. V., Vielmo, H. A., Petry, A. P., 2012. A review on the performance of savonius wind turbines. *Renewable and Sustainable Energy Reviews* 16 (5), 3054 – 3064.
- Alder, G., 01 1979. The aerodynamic performance of the savonius rotor 2, 119–126.
- Aliferis, A. D., Jessen, M. S., Dec. 2017. Performances of vertical axis wind turbines, lift type & drag type, project thesis at The Norwegian University of Science and Technology.
- Bardal, L. M., Sætran, L. R., 2017. Influence of turbulence intensity on wind turbine power curves. *Energy Procedia* 137, 553–558.
- Bartl, J., Sætran, L., 2017. Blind test comparison of the performance and wake flow between two in-line wind turbines exposed to different turbulent inflow conditions. *Wind Energy Science* 2 (1), 55–76.
- Bell, W., 1979. The influence of turbulence on drag. *Ocean Engineering* 6 (3), 329 – 340.
- Blackwell, B. F., Sheldahl, R. E., Feltz, L. V., 1978. Wind tunnel performance data for two- and three-bucket savonius rotors. Tech. rep., Sandia Laboratories, sand 76-0131 under act AT/29-11 Page 789.
- Brammer, J., Falconer, R., Kwan, A., 09 2013. Physical and numerical modelling of the wake characteristics of the savonius tidal stream turbine.
- Choukulkar, A., Pichugina, Y., Clack, C., Calhoun, R., Banta, R., Brewer, A., Hardesty, M., 2015. A new formulation for rotor equivalent wind speed for wind resource assessment and wind power forecasting. *Wind Energy*.
- Damak, A., Driss, Z., Abid, M., 2013. Experimental investigation of helical savonius rotor with a twist of 180 degrees. *Renewable Energy* 52 (Supplement C), 136 – 142.
- Draskovic, N., 2017. Measurement methods in turbulent flows. Master's thesis, Norwegian University of Science and Technology.
- Frikha, S., Driss, Z., Kchaou, H., Abid, M. S., 2016/09/12 2016. Incidence angle effect on the turbulent flow around a savonius wind rotor. *American Journal of Energy Research* 4 (2), 42–53, doi: 10.12691/ajer-4-2-3.
- Fujisawa, N., Gotoh, F., Aug. 1994. Experimental study on the aerodynamic performance of a savonius rotor. *J. Sol. Energy Eng* 116 (3), 148–152.



- 
- Haase, M., Skeie, K. S., Tronstad, T. V., 2014. Building integrated vertical wind turbines : Experiences from the roof of biskop gunnerus gate 14 in oslo. SINTEF Fag (19).
- Kumar, A., Saini, R., 2017. Performance analysis of a savonius hydrokinetic turbine having twisted blades. *Renewable Energy* 108, 502 – 522.
- Kumara, E., Hettiarachchi, N., Jayathilake, R., 08 2017. Review paper: Overview of the vertical axis wind turbines 4, 2313–3759.
- Loganathan, B., Mustary, I., Chowdhury, H., Alam, F., 2017. Effect of turbulence on a savonius type micro wind turbine. *Energy Procedia* 110, 549 – 554, 1st International Conference on Energy and Power, ICEP2016, 14-16 December 2016, RMIT University, Melbourne, Australia.
- Marmutova, S., 2016. Performance of a savonius wind turbine in urban sites using cfd analysis. Ph.D. thesis, University of Vaasa Faculty of Technology Energy Technology P.O. Box 700 FI-65101 Vaasa Finland.
- Pol, P. A. M., 06 2015. Tnumerical study of flow through a savonius wind turbine. Tech. rep.
- Rind, E., Castro, I. P., August 2012. On the effects of free-stream turbulence on axisymmetric disc wakes.
- Ross, I. J., 2010. Wind tunnel blockage corrections: An application to vertical-axis wind turbines. Master's thesis, University of Dayton.
- Rozenn, W., Ioannis, A., M., P. S., S., C. M., E., J. H., 2008. The influence of the wind speed profile on wind turbine performance measurements. *Wind Energy* 12 (4), 348–362.
- Saha, U., Rajkumar, M. J., 2006. On the performance analysis of savonius rotor with twisted blades. *Renewable Energy* 31 (11), 1776 – 1788.
- Schaffarczyk, A., Pawlak, M., Richert, F., 05 2018. New model for calculating intensities of turbulence in the wake of wind-turbines.
- Shamsoddin, S., Porté-Agel, F., Apr. 2017. A Large-Eddy Simulation Study of Vertical Axis Wind Turbine Wakes in the Atmospheric Boundary Layer. In: EGU General Assembly Conference Abstracts. Vol. 19 of EGU General Assembly Conference Abstracts. p. 13399.
- Shigetomi, A., Murai, Y., Tasaka, Y., Takeda, Y., 2011. Interactive flow field around two savonius turbines. *Renewable Energy* 36 (2), 536 – 545.
- Tian, W., Ozbay, A., Hu, H., 2014. Effects of incoming surface wind conditions on the wake characteristics and dynamic wind loads acting on a wind turbine model. *Physics of Fluids* 26 (12), 125108.

---

Torresi, M., Benedittis, F. A. D., Fortunato, B., Camporeale, S. M., 2014. Performance and flow field evaluation of a savonius rotor tested in a wind tunnel. *Energy Procedia* 45, 207 – 216, aTI 2013 - 68th Conference of the Italian Thermal Machines Engineering Association.

Zhang, B., Song, B., Mao, Z., Tian, W., 2017. A novel wake energy reuse method to optimize the layout for savonius-type vertical axis wind turbines. *Energy* 121, 341 – 355.

---

---

# Appendices



## A. More on the experimental set up

### Turbine

The Savonius turbine in this study was kindly donated by Getek AS in Trondheim. It is manufactured by a company called WindStream Technologies. The turbine is part of a product called TurboMill. Figure A.1 shows a TurboMill unit and also an example of how it can be installed on a roof top. One unit consists of three identical Savonius turbines



**Figure A.1:** *Left:* Assembled TurboMill unit, *Right:* TurboMill units installed on the roof of LACTEC Headquarters in Curitiba, Brazil September 2011. Both figures extracted from the TurboMill brochure by WindStream Technologies

mounted in series on generators. One TurboMill unit has an energy potential of 257kWh per year if the average wind speed is 5 m/s. It also has a rated power output of about 150W at wind speeds of 11m/s. The turbine has a helical twist so that the top is rotated 180 degrees relative to the bottom. It is also equipped with end plates. In this study, only one turbine was used. Many parts from the support structure of the TurboMill unit were reused and modified to fit the purpose of testing only one turbine. The turbine has diameter,  $D = 0.33\text{m}$ , is 0.99 meters tall and a projected frontal area of  $A = 0.327\text{ m}^2$ . For all measurements, the turbine was placed  $x/D = 13.6$  or 4.5 meters downstream of the test section inlet.

# Data Sheet: TurboMill



## TurboMill®

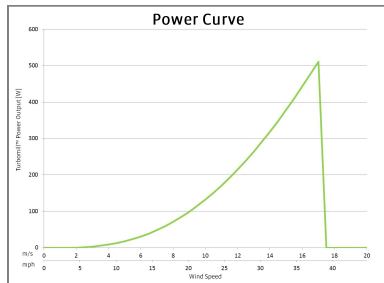
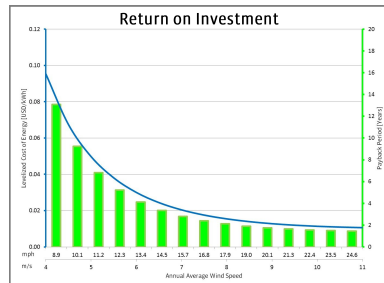
The affordable micro-wind energy system



### Installation Benefits

- Unique form factor, easily mounts to any building
- No complicated masts, guy wires, or towers
- Avoids engineering and permitting complexities
- Suitable for simple ballasted installation that avoids roof penetration
- Visually engaging design integrates with existing building architecture, custom colors available
- Durable construction, engineered for any environment
- Environmentally friendly, virtually silent

Technical Specifications	
Energy Potential (Per Unit)	257 kWh per year @ 5 m/s average wind speed
Rated Power Output	150 W @ 11 m/s
Maximum Power Output	500 W @ 17 m/s
Rotor Diameter	12.99 in   0.33 m
Cut-In Wind Speed	4.5 mph   2 m/s
Cut-Out Wind Speed	38.03 mph   17 m/s
Swept Area	1,519 in <sup>2</sup>   .980 m <sup>2</sup>
Survival Wind Speed	101 mph   45 m/s
TurboMill® Dimensions	51.18 in X 51.18 in X 25.197 in
Weight	82.3 lbs   37.33 kg
Turbine Material	Galvanized G-90 Steel
Corrosion Prevention	PPG Spectracron® 360 2K
Electrical Connection	On-Board Battery Charge Controller Grid-Tied Inverter (Optional)
Generator	Brushless, Permanent Magnet Generator
Design Life	20 Years



Dan Bates/CEO | dbates@windstream-inc.com | Mobile: 310-387-7636 | www.windstream-inc.com

# Data Sheet: Motor

# SIEMENS

## Data sheet for three-phase Squirrel-Cage-Motors



MLFB-Ordering data : 1LA7073-2AA10

without (standard)

Client order no. :  
Order no. :  
Offer no. :  
Remarks :

Item no. :  
Consignment no. :  
Project :

### Electrical data:

Rated voltage :	(1) 230 VDI/400 VY, 50 Hz, 460 VY, 60 Hz					
Frequency :	50 Hz		60 Hz			
Rated power :	0.55 kW		0.63 kW			
Rated speed :	2800 1/ min		3400 1/ min			
Rated torque :	1.9 Nm		1.8 Nm			
Rated current (IE) :	VD	VY	VY			
	2.37 A	1.36 A	1.36 A			
Starting / rated current :	4.3		4.9			
Breakdown / rated torque :	2.6		2.5			
Starting / rated torque :	2.5		2.6			
	4/4	3/4	2/4	4/4	3/4	2/4
Efficiency %	71.0%	71.0%	67.0%	71.0%	71.0%	67.0%
Power factor :	0.82	0.77	0.67	0.82	0.77	0.67
Efficiency class :	-		-			

### Mechanical data:

Sound pressure level 50Hz/60Hz (load) :	52 dB(A)	56 dB(A)
Moment of inertia :	0.00041 kg*m <sup>2</sup>	
Bearing DE :	6202 2ZC3	
Bearing NDE :	6202 2ZC3	
Type of bearing :	Floating bearings pre-loaded DE (standard)	
Condensate drainage holes :	No	
Regreasing device :	No	
Lubricants :	Esso Unirex N3	
Grease lifetime/Relubrication interval :	40000 h	
Quantity of grease for relubrication :	null g	
External earthing terminal :	No	
Coating :	Special paint finish RAL 7030 stone gray	

### Environmental conditions:

Ambient temperature :	-20 °C - +40 °C
Altitude above sea level :	1000 m
Standards and specifications :	IEC, DIN, ISO, VDE, EN

### General data:

Frame size	071 M
Design of rotating electrical machines :	(0) IM B3 / B6 / B7 / B8 / V5 without canopy
Weight in kg, without optional accessories :	6.00 kg
Frame material :	Aluminum
Degree of protection :	IP 55
Method of cooling, TEFC :	IC 411
Vibration class :	A (Standard)
Insulation :	155(F) to 130(B)
Duty type :	S1 - continuous duty
Direction of rotation :	Bi-directional

### Terminal box:

Material of terminal box :	Aluminum
Type of terminal box :	gk 030
Contact screw thread :	M4
Max. cross-sectional area :	1.50 mm <sup>2</sup>
Cable diameter from ... to ... :	9.00 mm - 17.00 mm
Cable entry :	1xM25x1,5-1xM16x1,5
Cable gland :	2 plugs

### Special design:

Technical data are subject to change! There may be discrepancies between calculated and rating plate values.

Generated: 06.12.2017 13:10:06



---

---

## B. Additional Contour Figures

### Mean cross stream and vertical velocity components

The normalized time-averaged crosswind velocity,  $\langle V \rangle / U_0$ , and normalized time-averaged vertical velocity,  $\langle W \rangle / U_0$ , are plotted in Figure B.1 and B.2, respectively. They both show an asymmetric wake behaviour as in the streamwise plot. There are however more dissimilarities between the cases in the plot for time-averaged crosswind velocity. For all scenarios but (A), there is a clear positive region of  $\langle V \rangle / U_0$  downstream of the turbine. This positive region is most likely due to the turbine giving the air a momentum in the opposite direction of the turbine rotation. The near absence of this region in case (A) is not obvious and should be investigated more closely, perhaps with a more accurate measurement technique. Interestingly, this near absence does however explain some of the increased overall asymmetry of the wake in case (A). With less momentum added by the turbine, the interaction between the strong and weak side of the wake decreases. Figure B.1 also shows that the wake is dominated by negative values of  $\langle V \rangle$ . The magnitude of these negative values seems to be affected by the rotational speed and direction of the turbine. These results are very plausible comparing them to streamlines of a rotating cylinder at different levels of rotational speed. Increasing the turbulence intensity of the incoming wind also seems to slightly reduce the magnitude of  $\langle V \rangle$ , since it induces more turbulent mixing in the wake.

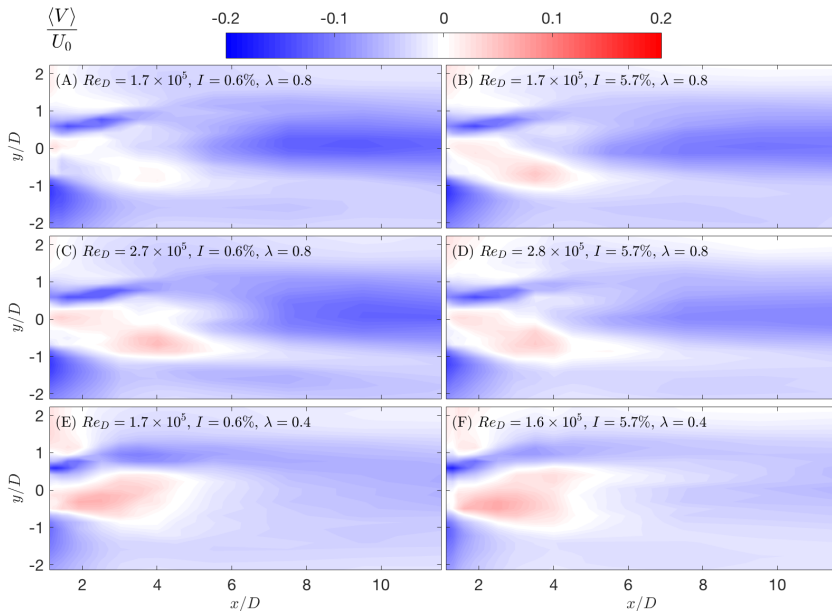


**Figure B.1:** Normalized contours of time-averaged cross-stream velocity of the wake in the x-y plane

Looking at Figure B.2, there are also asymmetries in the time-averaged vertical veloc-

ity component. The mid symmetry plane for a conventional Savonius turbine in uniform flow (with a symmetrical rig), would be expected to have about zero time-averaged vertical velocities. Hence, the non-trivial results in Figure B.2 can more or less be related to the helical shape of the rotor. Depending on the angular position of the blades, the airflow is either forced upwards or downwards. Again, there are evidently less differences and asymmetry in the cases of higher turbulence intensity. Without a vertical scan of the region downstream of the turbine, it is however difficult to provide any further investigation on the contributions of  $\langle W \rangle$  to the wake development.

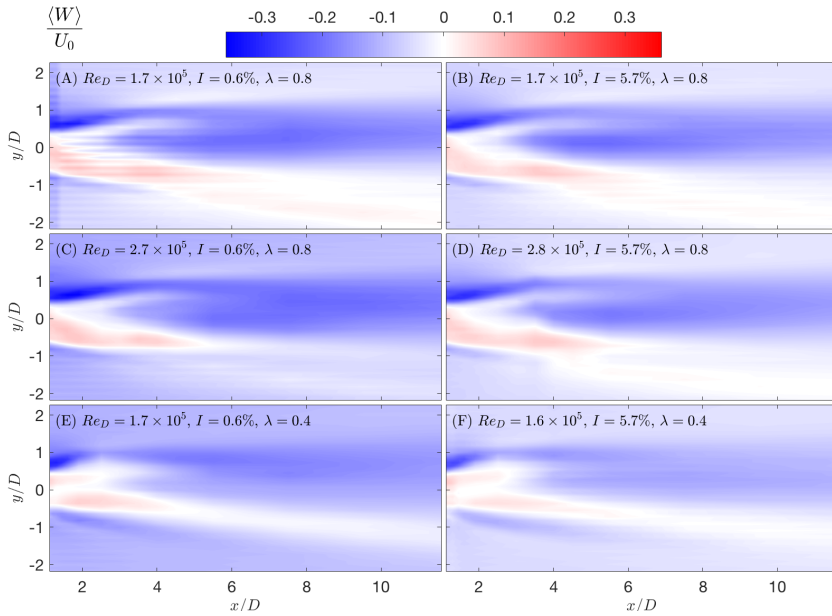


**Figure B.2:** Contours of normalized time-averaged vertical velocity of the wake in the x-y plane

## Components of turbulent kinetic energy

The streamwise, cross-streamwise and vertical component of turbulent kinetic energy is depicted in Figure B.3, B.4 and B.5, respectively. By examining these figures, the highest levels of turbulence are caused by streamwise fluctuations. The high magnitude in fluctuations in all components are concentrated near the turbine and thus no single component reaches particularly far away from the turbine.

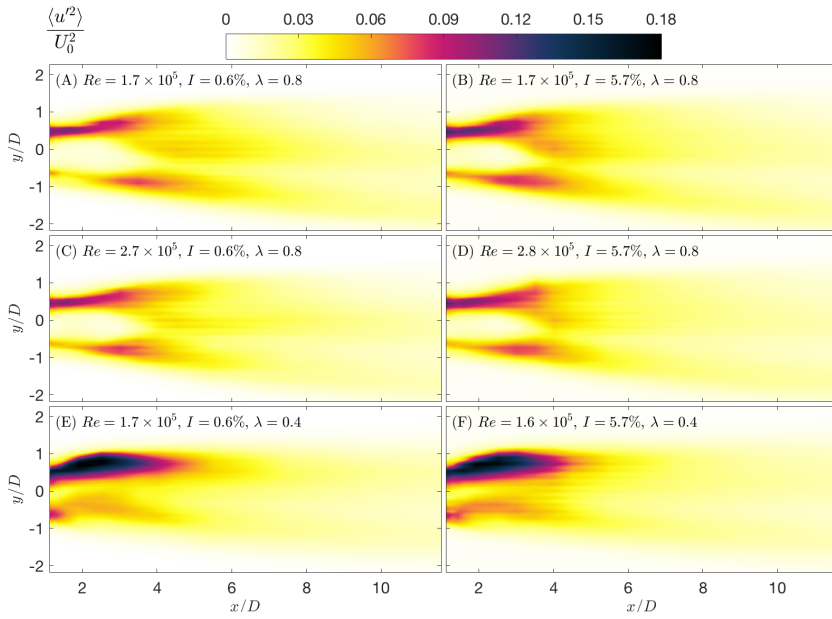


**Figure B.3:** Normalized contours of streamwise component  $\left(\frac{\langle u'^2 \rangle}{U_0^2}\right)$  of turbulent kinetic energy

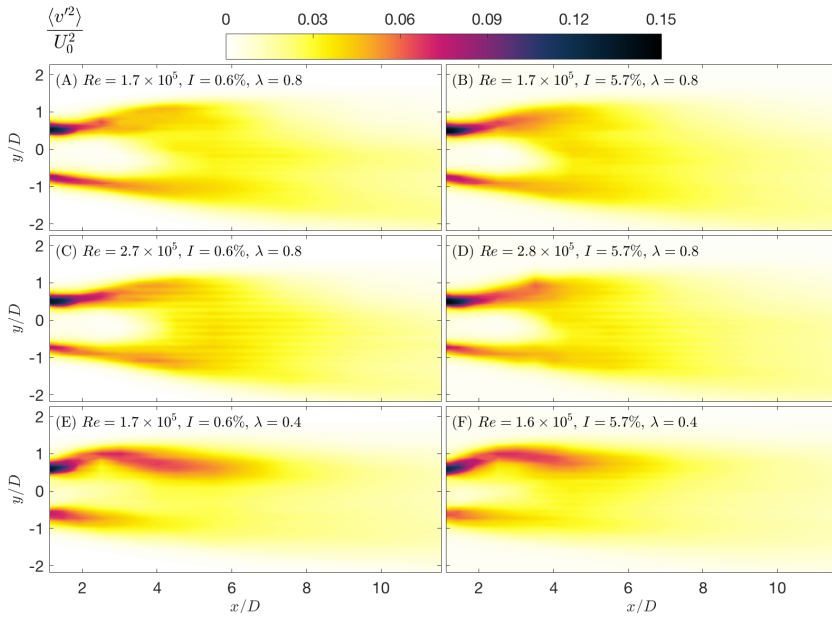


**Figure B.4:** Normalized contours of cross-streamwise component  $\left(\frac{\langle v'^2 \rangle}{U_0^2}\right)$  of turbulent kinetic energy

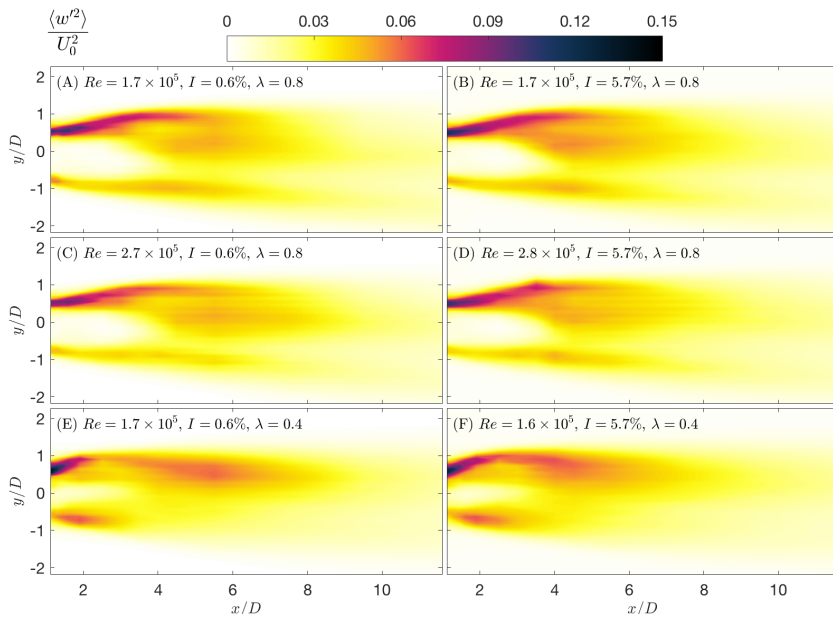


**Figure B.5:** Normalized contours of time-averaged vertical component  $\left(\frac{\langle w'^2 \rangle}{U_0^2}\right)$  of turbulent kinetic energy

## C. Turbulence Decay

The turbulence intensity in the wind tunnel decays downstream of the grid. Figure C.1 shows that the decay follows a power law,  $I = b \cdot (x/M)^m$ , where the coefficients  $b = 0.2571$  and  $m = -0.5836$ . The measured values are found in empty tunnel experiments.

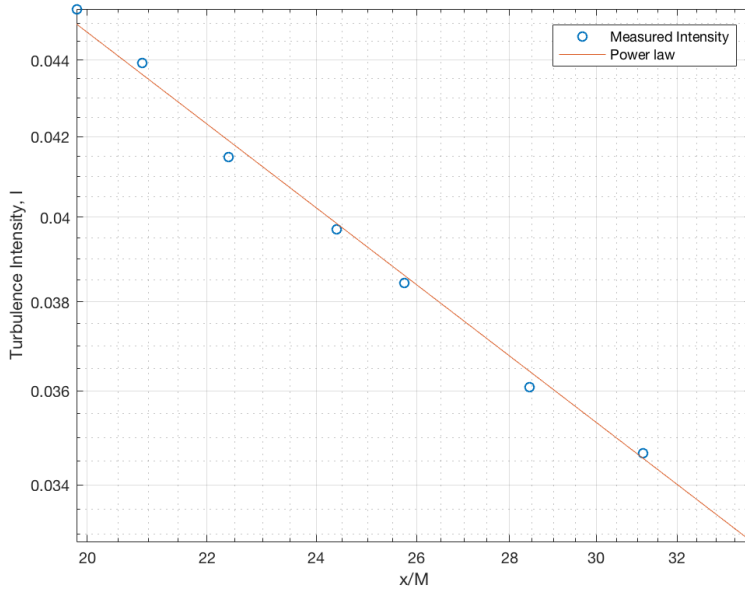


**Figure C.1:** Turbulence decay over the streamwise span of the measurement grid.  $M = 0.245\text{m}$  is the mesh size of the grid.  $x$  is the distance to the grid, which is placed at the inlet of the test section.



NTNU	<b>Risk assessment</b>	Prepared by	Number	Date	
		HSE section	HMSRV2603E	04.02.2011	
HSE/KS		Approved by		Replaces	
		The Rector		01.12.2006	

**Unit:** (Department) **EPT**

**Date:**

**Line manager:**

**Participants in the identification process** (including their function): Students: Alexander Dahl Aliferis and Marius Stette Jessen , Supervisor: R. Jason Hearst

**Short description of the main activity/main process:** Master project for students Alexander Dahl Aliferis and Marius Stette Jessen. Performance and wake measurements of a Savonius wind turbine

**Is the project work purely theoretical?** (YES/NO): NO

*Answer "YES" implies that supervisor is assured that no activities*

*requiring risk assessment are involved in the work. If YES, briefly describe the activities below. The risk assessment form need not be filled out.*

*requiring risk assessment are involved in the work. If YES, briefly describe the activities below. The risk assessment form need not be filled out.*

**Signatures:** Responsible supervisor: *R. J. Hearst*

Students: *Alexander D. Aliferis, Marius Stette Jessen*

Activity from the identification process form	Potential undesirable incident/strain	Likelihood:	Consequence:			Risk Value (human)	Comments/status Suggested measures
		Likelihood (1-5)	Human (A-E)	Environment (A-E)	Economy/material (A-E)		
01 Experimental setup.	Tripping and stumbling in equipments	4	A	A	A	A4	Turn on lights when needed. Use flashlight.
01 Experimental setup.	Heavy lifting, can lead to back injuries. Dropping equipment on the floor.	3	B	A	B	B4	Use proper lifting technique.
02 Wake Measurements in Wind Tunnel	Debris flying into eyes	3	B	A	B	B4	Use protection goggles

**Likelihood, e.g.:**

1. Minimal
2. Low
3. Medium
4. High
5. Very high

**Consequence, e.g.:**

- A. Safe
- B. Relatively safe
- C. Dangerous
- D. Critical
- E. Very critical

**Risk value (each one to be estimated separately):**

**Human = Likelihood x Human Consequence**

**Environmental = Likelihood x Environmental consequence**

**Financial/material = Likelihood x Consequence for Economy/material**



NTNU	<b>Risk assessment</b>	Prepared by	Number	Date	
		HSE section	HMSRV2603E	04.02.2011	
HSE/KS		Approved by		Replaces	
		The Rector		01.12.2006	

### **Potential undesirable incident/strain**

Identify possible incidents and conditions that may lead to situations that pose a hazard to people, the environment and any materiel/equipment involved.

### **Criteria for the assessment of likelihood and consequence in relation to fieldwork**

Each activity is assessed according to a worst-case scenario. Likelihood and consequence are to be assessed separately for each potential undesirable incident. Before starting on the quantification, the participants should agree what they understand by the assessment criteria:

#### **Likelihood**

Minimal 1	Low 2	Medium 3	High 4	Very high 5
Once every 50 years or less	Once every 10 years or less	Once a year or less	Once a month or less	Once a week

#### **Consequence**

Grading	Human	Environment	Financial/material
<b>E</b> Very critical	May produce fatality/ies	Very prolonged, non-reversible damage	Shutdown of work >1 year.
<b>D</b> Critical	Permanent injury, may produce serious health damage/sickness	Prolonged damage. Long recovery time.	Shutdown of work 0.5-1 year.
<b>C</b> Dangerous	Serious personal injury	Minor damage. Long recovery time	Shutdown of work < 1 month
<b>B</b> Relatively safe	Injury that requires medical treatment	Minor damage. Short recovery time	Shutdown of work < 1week
<b>A</b> Safe	Injury that requires first aid	Insignificant damage. Short recovery time	Shutdown of work < 1day


The unit makes its own decision as to whether opting to fill in or not consequences for economy/materiel, for example if the unit is going to use particularly valuable equipment. It is up to the individual unit to choose the assessment criteria for this column.

#### **Risk = Likelihood x Consequence**

Please calculate the risk value for "Human", "Environment" and, if chosen, "Economy/materiel", separately.

#### **About the column "Comments/status, suggested preventative and corrective measures":**

Measures can impact on both likelihood and consequences. Prioritise measures that can prevent the incident from occurring; in other words, likelihood-reducing measures are to be prioritised above greater emergency preparedness, i.e. consequence-reducing measures.

NTNU	Risk matrix	prepared by	Number	Date	
		HSE Section	HMSRV2604	8 March 2010	
HSE/KS		approved by	Page	Replaces	
	Rector	4 of 4	9 February 2010		

## MATRIX FOR RISK ASSESSMENTS at NTNU

<b>CONSEQUENCE</b>	Extremely serious	E1	E2	E3	E4	E5
	Serious	D1	D2	D3	D4	D5
	Moderate	C1	C2	C3	C4	C5
	Minor	B1	B2	B3	B4	B5
	Not significant	A1	A2	A3	A4	A5
		Very low	Low	Medium	High	Very high
		<b>LIKELIHOOD</b>				

Principle for acceptance criteria. Explanation of the colours used in the risk matrix.

Colour	Description
Red	Unacceptable risk. Measures must be taken to reduce the risk.
Yellow	Assessment range. Measures must be considered.
Green	Acceptable risk Measures can be considered based on other considerations.